









RESEARCH ARTICLE

# Attenuation of the extracellular matrix restores microglial activity during the early stage of amyloidosis

Stoyan Stoyanov<sup>1</sup>  | Weilun Sun<sup>1</sup>  | Henning Peter Düsedau<sup>2</sup>  |  
 Carla Cangalaya<sup>1,3</sup>  | Ilseob Choi<sup>1</sup> | Hadi Mirzapourdelavar<sup>1</sup> |  
 David Baidoe-Ansah<sup>1</sup>  | Rahul Kaushik<sup>1</sup>  | Jens Neumann<sup>4</sup> |  
 Ildiko Rita Dunay<sup>2,5</sup>  | Alexander Dityatev<sup>1,5,6</sup> 

<sup>1</sup>Molecular Neuroplasticity, German Center for Neurodegenerative Diseases (DZNE), Magdeburg, Germany

<sup>2</sup>Institute of Inflammation and Neurodegeneration, Medical Faculty, Otto-von-Guericke University, Magdeburg, Germany

<sup>3</sup>Institute of Biochemistry, Otto-von-Guericke University, Magdeburg, Germany

<sup>4</sup>Department of Neurology, Otto-von-Guericke University, Magdeburg, Germany

<sup>5</sup>Center for Behavioral Brain Sciences (CBBS), Magdeburg, Germany

<sup>6</sup>Medical Faculty, Otto-von-Guericke University, Magdeburg, Germany

## Correspondence

Alexander Dityatev, German Center for Neurodegenerative Diseases (DZNE), Leipziger Str. 44, Magdeburg 39120, Germany.  
 Email: alexander.dityatev@dzne.de

Ildiko Rita Dunay, Institute of Inflammation and Neurodegeneration, Medical Faculty, Otto-von-Guericke University, Magdeburg D-39120, Germany.  
 Email: ildiko.dunay@med.ovgu.de

## Funding information

China Scholarship Council, Grant/Award Number: 201406170032; Deutsche Forschungsgemeinschaft, Grant/Award Numbers: 2413/1 TP5, 2413/1 TP6; European Structural and Investment Funds, Grant/Award Number: ZS/2016/08/80645

## Abstract

In the advanced stages of Alzheimer's disease (AD), microglia are transformed to an activated phenotype with thickened and retracted processes, migrate to the site of amyloid-beta (A $\beta$ ) plaques, and proliferate. In the early stages of AD, it is still poorly understood whether the microglial function is altered and which factors may regulate these changes. Here, we focused on studying microglia in the retrosplenial cortex (RSC) in 3- to 4-month-old 5xFAD mice as a transgenic mouse model of AD. At this age, there are neither A $\beta$  plaques, nor activation of microglia, nor dysregulation in the expression of genes encoding major extracellular matrix (ECM) molecules or extracellular proteases in the RSC. Still, histochemical evaluation of the fine structure of neural ECM revealed increased levels of *Wisteria floribunda* agglutinin labeling in holes of perineuronal nets and changes in the perimeter of ECM barriers around the holes in 5xFAD mice. Two-photon vital microscopy demonstrated normal morphology and resting motility of microglia but strongly diminished number of microglial cells that migrated to the photolesion site in 5xFAD mice. Enzymatic digestion of ECM by chondroitinase ABC (ChABC) ameliorated this defect. Accordingly, the characterization of cell surface markers by flow cytometry demonstrated altered expression of microglial CD45. Moreover, ChABC treatment reduced the invasion of myeloid-derived mononuclear cells into the RSC of 5xFAD mice. Hence, the migration of both microglia and myeloid cells is altered during the early stages of amyloidosis and can be restored at least partially by the attenuation of the ECM.

## KEYWORDS

Alzheimer's disease, amyloidosis, chondroitinase ABC, extracellular matrix, microglia, neuroinflammation, retrosplenial cortex

Stoyan Stoyanov and Weilun Sun contributed equally to this study.

This is an open access article under the terms of the Creative Commons Attribution-NonCommercial License, which permits use, distribution and reproduction in any medium, provided the original work is properly cited and is not used for commercial purposes.

© 2020 The Authors. GLIA published by Wiley Periodicals LLC

## 1 | INTRODUCTION

The mammalian central nervous system (CNS) possesses a unique immune defense mechanism to protect itself from invading pathogens and other toxic agents. Arising from yolk sac macrophages, brain microglial cells play a critical role not only in maintaining the innate immune response, but also in shaping the healthy neuropil through a number of different functions (Ginhoux et al., 2010). During development, microglia are thought to contribute to neuronal proliferation and differentiation in addition to the pruning of apoptotic and excess neurons. During adulthood, microglial cells participate in active synaptic remodeling and the clearance of weak synapses as well as in the phagocytosis of cellular debris and aberrant proteins (Paolicelli et al., 2011; Sierra et al., 2010; Stevens et al., 2007; Tremblay, Lowery, & Majewska, 2010; Wagner, Kim, Savall, Schnitzer, & Luo, 2017). Microglia are the major resident players in neuroinflammatory processes, however, also the infiltration of monocytes and neutrophils may occur in response to particular neurodegenerative stimuli and thus contribute to a more complex immune response (Biswas et al., 2015; Biswas et al., 2017; Dusedau et al., 2019). Microglia, together with recruited peripheral immune cells, are able to promote neuronal damage and loss as well as contribute to neurogenesis (Mohle, Israel, et al., 2016; Mohle, Mattei, et al., 2016; Neumann et al., 2015). Infiltration may occur in cases of pathologically compromised blood–brain barrier (BBB) function, as observed not only during aging, but also during mild cognitive impairment and dementia (Farfara et al., 2019; Montagne et al., 2015; van de Haar et al., 2016; Zlokovic, 2005). The most common pathologic condition of the CNS that leads to dementia is Alzheimer's disease (AD). One hallmark of AD is amyloidosis, that is, the increased deposition of peptides originating from the proteolytic processing of amyloid- $\beta$  (A $\beta$ ) precursor protein (APP) by  $\beta$ - and  $\gamma$ -secretases. The overproduction of A $\beta$ , together with impaired clearance through the BBB, results in an immense excess of aggregate-prone A $\beta$  peptides in the brain neuropil, which give rise to a number of neurotoxic A $\beta$  fragments and protofibrillar hotspots (Thinakaran & Koo, 2008). It has been shown extensively that the accumulation of the A $\beta$  peptide facilitates neuronal injury and perpetuates neurodegenerative damage (Hofrichter et al., 2013; Palop, Chin, & Mucke, 2006). However, the number of senile plaques has been poorly correlated with the degree of clinical dementia in patients, further showing that monomeric and oligomeric A $\beta$  species independently trigger a cascade of downstream events contributing to a synaptic loss (Lue et al., 1999). Microglial cells are recruited to the microregions of A $\beta$  hotspots to influence outward expansion by the expression and secretion of several inflammatory mediators, such as cytokines, chemokines, inflammasomes, and reactive oxygen species (ROS; Heneka et al., 2013; Nimmerjahn, Kirchhoff, & Helmchen, 2005). Microglia adopt an activated phenotype with an amoeboid cell body shape and begin the engulfment of A $\beta$  fragments. The microglial envelopment of protofibrillar A $\beta$  plaques and collateral neurotoxicity expand with age (Bolmont et al., 2008; Condello, Yuan, Schain, & Grutzendler, 2015; Meyer-Luehmann et al., 2008). Despite the enormous progress that has been made in

the last few years, there is still no clear understanding of how the early pathology and progression of AD, which includes memory loss and neural circuit disruption, are linked to microglial phenotype and function.

Animal studies have demonstrated impairment in hippocampal long-term potentiation and contextual memory formation in the early stages of amyloidosis before the onset of A $\beta$  plaque formation (Do Carmo & Cuello, 2013; Marchetti & Marie, 2011). Interestingly, this stage is characterized by an overexpression of extracellular matrix (ECM) molecules (Vegh et al., 2014). The neural ECM is formed by the aggregation of multiple molecules synthesized and secreted by neurons and glial cells. The interaction between the ECM and the neural cells in the developing brain plays a crucial role in cell migration and the guidance of the growing axons, but the formation of the mature neural ECM, for instance in the form of perineuronal nets (PNNs) associated with fast-spiking interneurons, is believed to restrict certain forms of structural developmental plasticity (Fawcett & Asher, 1999; Jones, Yamaguchi, Stallcup, & Tuszyński, 2002; Kwok, Dick, Wang, & Fawcett, 2011; Pyka et al., 2011). On the other hand, several major components of the neural ECM are required for the induction of functional plasticity in the mature brain (Kochlamazashvili et al., 2010). Accumulating evidence suggests that ECM molecules may play causal and modulatory roles in the pathogenesis of various CNS diseases (Soleman, Filippov, Dityatev, & Fawcett, 2013). A significant increase in the levels of the chondroitin sulfate proteoglycans (CSPGs) neurocan and brevican as well as in the concentration of the proteoglycan crosslinking proteins tenascin-R and hyaluronan/proteoglycan link protein 1 (HAPLN1) have been detected in 3-month-old APP<sup>swe</sup>/PS1<sup>dE9</sup> (APP/PS1) mice (Vegh et al., 2014). Enzymatic treatment with chondroitinase ABC (ChABC), which degrades glycosylated sugar chains of CSPGs and thus attenuates the neural ECM, restores cognitive impairment and long-term potentiation in an animal model of AD (Vegh et al., 2014). The removal of CSPGs via ChABC digestion also promotes cortical plasticity, specifically the experience-dependent generation and rearrangement of synaptic connections in the visual cortex, as reported by Pizzorusso and colleagues (Pizzorusso et al., 2002). The delivery of ChABC *in vivo* has been shown to confer much of the inhibitory properties of CSPGs at the state of inflammation (Bartus et al., 2014). In spinal cord injury, these neuroprotective effects lead to long-term improved functional outcomes and reveal novel mechanistic evidence of the macrophage phenotype modulation underlying these conditions (Didangelos, Iberl, Vinsland, Bartus, & Bradbury, 2014).

The retrosplenial cortex (RSC) forms a reciprocal network with the hippocampus, thalamus and amygdala and is involved in spatial learning, navigation and emotional memory formation, and extinction (Pothuizen, Davies, Aggleton, & Vann, 2010; Sugar, Witter, van Strien, & Cappaert, 2011; van de Haar et al., 2016). The RSC is affected by A $\beta$  in the very early stages of AD before the appearance of clinical symptoms (Frisoni et al., 2007; Pengas et al., 2012). Here, we aimed to study the role of the microglia-ECM interaction in the RSC in an early stage of amyloidosis and investigated the physiological activity of microglia and their activation. To address this issue, we

performed in vivo imaging and flow cytometric analysis of microglia in 3- to 4-month-old 5x*FAD* mice with and without ChABC treatment.

## 2 | MATERIALS AND METHODS

### 2.1 | Animals

We used 3- to 4-month-old male CX3CR1<sup>gfp/+</sup> (B6.129P-Cx3cr1<sup>tm1Litt</sup>/J, Stock No: 005582) mice with microglia expressing enhanced green fluorescent protein (EGFP) under the control of the endogenous *Cx3cr1* locus (Jung et al., 2000). To investigate the dynamic properties of microglia and the mechanisms underlying their activation upon the introduction of a laser-induced lesion in a model of AD, we crossbred the CX3CR1<sup>gfp/+</sup> mice with 5x*FAD*<sup>+/-</sup>. Bl6 (B6.CgTg(APPswFILon,PSEN1\**M146L*\**L286V*)6799 Vas/MmJ-ax, Stock No: 34848-JAX) mice, which overexpress human APP695 with KM670/671/NL (Swedish), V717I (London) and I716V (Florida) mutations and human PS1 harboring M146L and L286V mutations under the Thy1 promoter, as described elsewhere (Oakley et al., 2006). All mice strains were purchased from The Jackson Laboratory, Bar Harbor, Maine, USA, and colonies were bred in the animal facility of the DZNE site in Magdeburg, Germany. We confirmed that the EGFP signal represents microglia cells in the RSC of these mice by ex-vivo immunostaining of microglia specific marker TMEM-119 (Figure S1). All animals were treated in strict accordance with ethical animal research standards defined by German law and approved by the Ethical Committee on Animal Health and Care of the State of Saxony-Anhalt, Germany (license number: 42502-2-1244). Light-reared animals were housed under a fixed 12-hr light/dark cycle.

### 2.2 | Surgical procedures

Surgeries were performed as described previously (Holtmaat et al., 2009; Senkov et al., 2006). The mice were briefly sedated with isoflurane in a chamber, and their heads were fixed in a stereotaxic apparatus (SR-6M, Narishige Scientific Instrument Lab, Japan). Once the heads were fixed, the isoflurane levels were adjusted first to 4% for induction and then to 1.5–2%, the oxygen levels were set to 0.4 L/min, and the depth of anesthesia was monitored by the breathing rate. Body temperature was maintained at 37°C using a heating pad connected to a temperature controller (ATC1000, World Precision Instruments, USA). Ketoprofen (5 mg/kg of body weight) was injected intraperitoneally before surgery to prevent inflammation and pain. Ophthalmic ointment was applied to protect the eyes during surgery. After the skin was cleaned with 70% ethanol and the hair was shaved, an approximately 8-mm<sup>2</sup> cutaneous incision was made, and then a 5 mm diameter craniotomy was gently performed over the RSC by a high-speed dental drill (Eickemeyer, Germany). After opening a cranial window, an intracerebral infusion (one per hemisphere) of 200 nL of either 50 U/mL ChABC (AMS.E 1028-10, AMSIBIO, Europe) in phosphate-buffered saline (PBS) with 0.1% bovine serum

albumin (BSA) or vehicle (PBS with 0.1% BSA) was administered into the RSC (AP: −2.0 mm; ML: 0.5 mm; DV: 0.5 mm) with a 10 µl NanoFil syringe (World Precision Instruments, USA) using an Ultra Micro Pump (UMP3, World Precision Instruments, USA). A cranial cranial glass window (Thermo Fisher Scientific, 6.0 mm diameter) was then fixed in place by applying superglue (Roti Coll-1, Carl Roth, Germany) to the edges and then sealed with dental cement (Paladur, Heraeus Kulzer, Germany). After all procedures, the animals were placed in a recovery chamber for 24 hr and given postoperative analgesia (ketoprofen, 5 mg/kg of body weight).

### 2.3 | Two-photon in vivo microscopy

The animals were divided into four groups of 5 mice according to genotype (CX3CR1<sup>gfp/+</sup> x 5x*FAD*.Bl6<sup>+/-</sup> or CX3CR1<sup>gfp/+</sup> x 5x*FAD*.Bl6<sup>-/-</sup> mice) and treatment (injection of ChABC or vehicle into the RSC 24 hr before imaging). Two-photon imaging and laser ablation protocols were modified from those used in previous studies (Davalos et al., 2005; Nimmerjahn et al., 2005). Immediately before imaging, the mice were anesthetized intraperitoneally with ketamine (90 mg/kg of body weight) and xylazine (18 mg/kg of body weight) in a 0.9% NaCl solution and placed in a custom-made head fixation frame, and body temperature was maintained at 37°C with a heating pad. Thirty minutes after the initial anesthesia, an ~1% isoflurane/O<sub>2</sub> gas mixture was employed to maintain anesthesia during the imaging procedures. The retrobulbar application of 100 µl of rhodamine-dextran (10 mg/ml in PBS) was performed before every imaging session to label the brain vasculature, and methoxy-X04 (2 mg/kg of body weight) was applied 5 min before the first imaging session to confirm that no Aβ plaques were formed at the studied age (Figure S2). All mice were chronically imaged for three consecutive days (2.5–3.5 hr daily) (Figure 1a,b). A multiphoton microscope (LSM 7 MP, Carl Zeiss, Germany) with a Ti:sapphire laser set to 850 and 760 nm wavelengths was used for transcranial imaging. To minimize phototoxicity, the average excitation laser power was kept at the minimum required to produce a sufficient signal-to-noise ratio. Fluorescence was detected using BP-420-480, BP 500-550, and BP 565-610 filters. A water immersion objective (×20, N.A. = 1.0, Carl Zeiss, Germany) was used throughout the imaging sessions. To address microglial morphology and dynamics in the resting state, we performed a time-lapse (50 frames, 20 s interframe interval) acquisition of z-stacks (6 optical sections with an interval of 3.5 µm) 150–200 µm below the pial surface 24, 48, and 72 hr after treatment with ChABC or vehicle. Immediately after each resting state recording, we applied a single microglia cell laser ablation (SMCLA) technique to induce a highly precise and reproducible local injury. SMCLA was achieved by focusing a two-photon laser beam at a single cell in the RSC located ~150–200 µm below the pial surface. The wavelength of the two-photon laser was set to 850 nm, and the laser power was adjusted to ~150–200 mW at the target (Davalos et al., 2005). The laser beam was focused at the target position for ~0.5 s to achieve the highest precision photodamage. The final damage area was determined by a relatively bright autofluorescent sphere

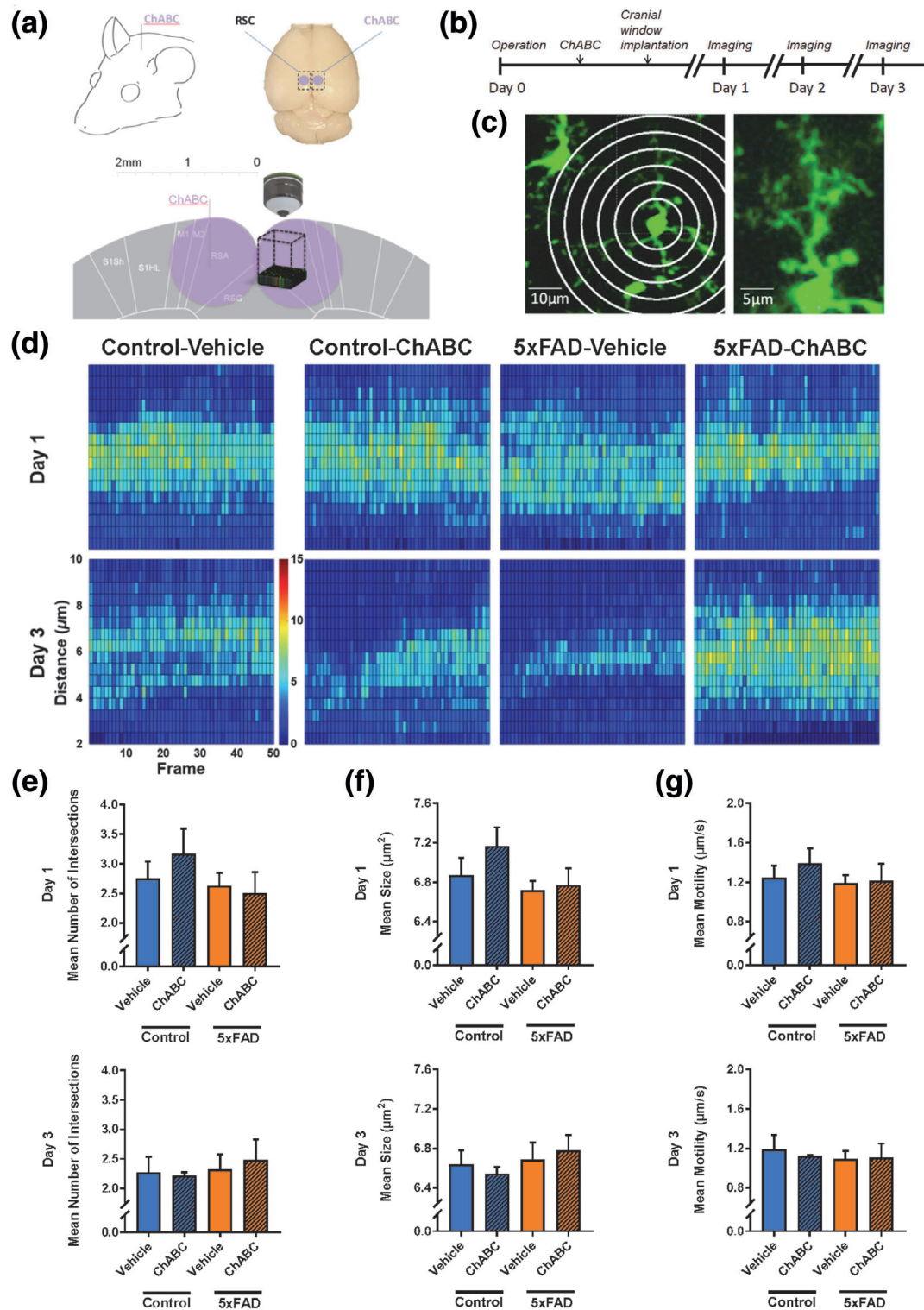


**FIGURE 1** Basal microglia motility and complexity are not affected by ChABC and in 5xFAD mice. (a) Scheme of ChABC intracerebral injection into RSC and imaging. (b) Time course of all procedures. (c) Sholl analysis of single microglia cell motility in vivo. (d) Color codes of microglia intersection number at a defined distance from the soma (diameter) in CX3CR1<sup>flp+/−</sup> × 5xFAD.B16<sup>−/−</sup> (for simplicity, denoted as control) and CX3CR1<sup>flp+/−</sup> × 5xFAD.B16<sup>+/−</sup> (for simplicity, denoted as 5xFAD) mice after vehicle / ChABC treatment. (e) Plots of the mean intersection numbers from single microglia cells (n = 4 animals) for Day 1 and Day3 after treatment of control and 5xFAD mice. Microglia single-cell measurements for size and motility are plotted in (f and g). No difference between groups was detected by two-way ANOVA (n = 4/5 mice; mean ± SEM values are shown) [Color figure can be viewed at wileyonlinelibrary.com]





around the focal point of the beam. For each time point and each brain hemisphere, we targeted three single microglia cells and then performed a time-lapse (100 frames, 20 s interval) acquisition of z-stacks (six optical sections with an interval of 3.5  $\mu\text{m}$ ).

## 2.4 | Cell isolation from RSC

Immune cell isolation from the brains of the mice was performed as described previously (Dusedau et al., 2019). Briefly, dissected brain samples containing the RSC were homogenized in a buffer containing 1 M HEPES (pH 7.3, Thermo Fisher Scientific, Waltham, MA) and 45% glucose before being sieved through a 70- $\mu\text{m}$  cell strainer. The homogenate was fractionated on a discontinuous 30–70% Percoll gradient (GE Healthcare, Chicago, IL), and the collected cells were washed in PBS and used subsequently for flow cytometric analysis.

## 2.5 | RNA extraction, cDNA conversion, and qPCR

From cortical and retrosplenial cortical regions of 5xFAD and control mice, total RNA was extracted using the EURx GeneMatrix DNA/RNA Extracol kit (Roboklon, Cat. No. E3750) according to the manufacturer's recommendations (Baidoe-Ansah et al., 2019; Ventura Ferreira et al., 2018). RNA products were further checked for genomic DNA contamination by using Nano-drop and gel electrophoresis to measure RNA yield, purity and integrity respectively. Then, 1.5  $\mu\text{g}$  of RNA was taken for cDNA conversion using the High-Capacity cDNA Reverse Transcription Kit (Cat. No. 4368814). Using the QuantStudio 5 (Applied Biosystems) or LightCycler® 96 (Roche) and following manufacturer's recommendations, qPCR analyses were performed with TaqMan™ gene expression assay (ThermoFisher Scientific, Cat. No. 4331182) or Power SYBR® Green RNA-to-CT™ 1-Step Kit (ThermoFisher Scientific, Cat. No. 4389986). Details of all TaqMan™ probes used are given in Table S1. Self-designed primers utilized in the SYBR® Green RT-qPCR (see Table S2) were synthesized by TIB MOLBIOL (Germany) and used at 100 nM final concentration (Figueiredo et al., 2019). Finally, gene expression per sample was normalized relative to expression of glyceraldehyde 3-phosphate dehydrogenase (*Gapdh*) or hypoxanthine-guanine phosphoribosyltransferase.

## 2.6 | Flow cytometric analysis

For the flow cytometric analysis of cell phenotypes, the cells were first incubated with ZOMBIE NIR™ fixable dye (Biolegend, San Diego, CA) for live/dead discrimination. To prevent the nonspecific binding of the antibodies, an anti-Fc $\gamma$ III/II receptor antibody (clone 93) was applied to the cells before staining for cell surface markers with fluorochrome-conjugated antibodies in FACS buffer (PBS containing 2% fetal bovine serum and 0.1% sodium azide). CD45 (30-F11), CD11b (M1/70), MHC class I (28-14-8), and CD11c (N418) antibodies

were all purchased from eBioscience (San Diego, CA); a CD29 (9EG7) antibody was derived from BD Biosciences (Franklin Lakes, NJ).

The cells were acquired using a BD FACS Canto II flow cytometer, and the obtained data were analyzed using the FlowJo software (Version 10, FlowJo LLC, Ashland, OR, USA). Fluorescence Minus One (FMO) controls were used to determine the autofluorescence in the respective detection channel.

## 2.7 | Histochemistry

Three days after ChABC or vehicle injection, or naïve animals were deeply anesthetized using ketamine (90 mg/kg of body weight) and xylazine (18 mg/kg of body weight) in a 0.9% NaCl solution and perfused transcardially with 4% PFA containing PBS. The dissected brains were incubated in 4% PFA containing PBS, cryoprotected in 30% sucrose containing phosphate buffer (PB) solution for 48 hr and frozen in 100% 2-methylbutan at  $-80^{\circ}\text{C}$ . Slices of 50- $\mu\text{m}$ -thick coronal sections were kept floating in solution (1 part ethylene glycol, 1 part glycerin, 2 parts PBS, pH = 7.2) at  $4^{\circ}\text{C}$ . At least five RSC sections per animal were selected for staining. All sections were washed in 120 mM phosphate buffer (PB), pH = 7.2. For *Wisteria floribunda* agglutinin (WFA) staining, freely floating RSC sections were permeabilized with PB containing 0.5% Triton X-100 (Sigma, T9284) for 10 min at room temperature (RT), followed by the application of a blocking solution (PB supplemented with 0.3% Triton X-100 and 5% normal goat serum, NGS, Gibco, 16210-064) for 1 hr at RT. Afterward, the sections were incubated for 48 hr ( $4^{\circ}\text{C}$ ) with biotinylated WFA (1:500, Vector Laboratories, B-1355) or anti-human Amyloid-beta (N) (82E1, 1:250, IBL, 10303), anti-TMEM-119 (1:300, abcam, ab209064), or rabbit anti-parvalbumin (1:300, SWANT Swiss Antibodies, PV27). The sections were then washed 3 $\times$  10 min at RT in PB and incubated on a shaker for 3 hr at RT with the secondary reagents: streptavidin Alexa Fluor® 546 (1:400, Thermo Fisher Scientific, S11225) or goat anti-mouse Alexa Fluor® 405 (1:500, Invitrogen, A31553) or goat anti-rabbit Alexa Fluor® 546 (1:500, Invitrogen, A11035), or goat anti-rabbit Alexa Fluor® 405 (1:500, Invitrogen, A31556). The sections were then washed with PB and stained with Hoechst 3342 (1 mg/mL in DMSO, 1:500 dilution, Sigma, B2261) before being mounted on Superfrost glasses with Fluoromount (Sigma, F4680). Confocal microscopy was performed with a Zeiss LSM 700 microscope.

## 2.8 | Data acquisition, processing, and analysis of time-lapse recordings

Stacks of multiphoton microscopic images were acquired from  $424.27 \times 424.27 \mu\text{m}$  areas in the RSC (see above) for approximately 2000 s. A single imaging data set consisted of 100 frames with 6 z-stacks; each frame had a  $512 \times 512$  pixel image resolution. We used a MATLAB-based semiautomated image analysis technique and an ImageJ-based Sholl analysis plugin. The isolated regions of interest

(ROIs) from the imaging data set were processed to track the dynamics of the microglial cells (e.g., velocity) using a customized histogram equalization algorithm in MATLAB. For each frame, the distance of the leading edge of the microglial processes in the photolesion site was computed using a local maximum fluorescence intensity (MFI) for 20 directions. Single microglial cell complexity and size as well as baseline motility were calculated for individual microglial cells using Sholl analysis (Sholl, 1953). The cell complexity index was defined as the mean number of intersections between a microglial cell and spheres of increasing radii averaged over time and radius length, that is, as  $\frac{1}{FD} \sum_{i=1}^F \sum_{j=1}^D n_{ij}$ , where  $F$  stands for the number of frames;  $D$  is the number of radii ( $r_j = j * \Delta r$ , with  $\Delta r = 2 \mu\text{m}$ ); and  $n_{ij}$  is the number of intersections between the microglial processes in the  $i$ -th frame and a sphere with a radius  $r_j$ . Additionally, the cell size was defined by measuring the distance from the cell body at which the intersections are located, that is,  $\frac{1}{FD} \sum_{i=1}^F \sum_{j=1}^D r_j * n_{ij}$ . Finally, the baseline motility was defined as the standard deviation from the mean profile of the intersections  $n_j$  (averaged over all frames), that is,  $\sqrt{\frac{1}{FD} \sum_{i=1}^F \sum_{j=1}^D (n_{ij} - n_j)^2}$ .

Furthermore, to address the gross changes at a single time point, we plotted the mean density of the intersections between radius length in the Sholl analysis, that is, the radius length as determined by  $d_i = \frac{\sum_{j=1}^D n_{ij}}{D}$ , where  $d_i$  depicts the mean density of intersections in the  $i$ -th frame,  $D$  is the number of radii;  $i$  stands for the index of the frame number; and  $n_{ij}$  is the number of intersections of microglial cell activation in the  $i$ -th frame with a sphere with a given radius length. The velocity of microglial processes toward laser damage was defined as the mean distance traveled over all 20 directions as described above.

## 2.9 | Image acquisition and histochemical measurements

To count the PNN-positive (PNN+) and parvalbumin-immunopositive (PV+) cells, one image per animal was taken in the dysgranular RSC using Zeiss LSM 700 confocal microscope equipped with EC Plan-Neofluar 10x/0.30 M27 objective (16-bit, 12 optical sections, 3.687  $\mu\text{m}$  intervals between sections, 1,024  $\times$  1,024 pixels, the pixel size of 0.625  $\mu\text{m}$ ). Image analysis was performed by an experimenter blind to the experimental conditions. The number of PV+/PNN+, PV+/PNN-, PV-/PNN+, and CX3CR1+ cells, and the area, PV intensity and circularity of PV+/PNN+ and PV-/PNN+ cells, as well as the soma area of CX3CR1+ cells were measured on the maximum intensity z-projection images using custom made Fiji scripts.

High-resolution images of PNNs for fine structure analysis were acquired using Zeiss LSM 700 confocal microscope and E Plan-Apochromat 63x/1.40 oil M27 objective, while the experimenter was blinded to the treatment group. For each animal, 5–7 images of PV + WFA+ cells per animals were acquired in the dysgranular RSC (16-bit, 14 optical sections, 0.170  $\mu\text{m}$  intervals between sections, 1,024  $\times$  1,024 pixels, the pixel size of 0.099  $\mu\text{m}$ ).

To measure the properties of PNN units (holes and ECM barriers around them), we developed a Fiji script APNU v1.2 (stands for Analysis of Perineuronal Net Units). The program prompts the user to choose a centrally located pixel within each of PNN holes and then provides automatic outlines of the holes as areas where the ECM intensity remains lower than the mean intensity at the hole center plus a given threshold (the same for compared groups). Then, the coordinates of the hole center are re-defined using the center of mass of the outlined hole (this is the only difference as compared to the published version of APNU v1.1 by (Kaushik et al., 2020). Afterward, the program computes profiles of ECM intensity along with the given number of tracking directions (20 sectors in this study) from the hole center for a given number of confocal layers (three in this study) in which a PNN unit is expected to be located. The ECM barrier coordinates are defined by local maxima in ECM intensity in a plane where the hole center is located (2D ECM) or by 3D coordinates corresponding to the maximal intensities for each of tracking directions (3D ECM; Kaushik et al., 2020).

## 2.10 | Statistical analysis

To compare the microglial parameters between the two genotypes and the two treatments each day, we applied two-way ANOVA followed by post hoc one-way ANOVA or multiple comparison tests using the Student–Newman–Keuls method. Similarly, the influence of time, treatment and genotype were compared using three-way ANOVA. All statistical analyses were performed with a 5% significance level using R 3.4.1, XLSTAT, and GraphPad Prism 6 (San Diego, CA).

## 3 | RESULTS

### 3.1 | ChABC injection leads to the digestion of PNNs in the retrosplenial cortex

To investigate how the attenuation of ECM may regulate microglial behavior in vivo, we intracranially injected ChABC or vehicle into the RSC of adult 3- to 4-month-old mice. It has been shown that a single injection of ChABC results in the long-lasting attenuation of the ECM in the target region (Bruckner et al., 1998; Lin, Kwok, Crespo, & Fawcett, 2008). To verify the attenuation of the ECM in our experimental setup, we performed histochemical staining with biotinylated *Wisteria floribunda* agglutinin (WFA), which specifically labels the *N*-acetylgalactosamine moiety of CS glycosaminoglycans (CS-GAGs) in the PNNs of perfused and fixed brains (Hartig et al., 1999; Steindler & Cooper, 1986). There was intense WFA labeling around inhibitory PV+ interneurons in the RSC of the animals injected with the vehicle. The bilateral in vivo application of ChABC caused a strong reduction in WFA-labeling 72 hr after injection (Figure S3). Thus, the intracranial injection of ChABC into the RSC in vivo induces the long-term digestion of PNNs (for at least three

consecutive days) and allows us to evaluate microglial dynamics upon the attenuation of the ECM.

### 3.2 | Basal microglial motility and complexity are not affected by attenuation of ECM and amyloidosis

To study in detail the functional significance of the ECM-microglia interaction, we performed two-photon imaging of the microglia in the RSC over 3 days in anesthetized 3- to 4-month-old CX3CR1<sup>gfp+/-</sup> × 5xFAD.B16<sup>-/-</sup> (for simplicity, denoted as control) and CX3CR1<sup>gfp+/-</sup> × 5xFAD.B16<sup>+/-</sup> (for simplicity, denoted as 5xFAD) mice (Figure 1a,b). Our time-lapse recording (50 frames with an ~20 s interframe interval) of EGFP-expressing microglia revealed the continuous movement of single microglial cell processes under basal conditions (Video S1). In addition, no plaques were identified *in vivo* in RSC using methoxy-X04 marker (Figure S2), and this evidence was confirmed by *ex vivo* immunostaining for A $\beta$ , which accumulations were detectable in the hippocampus but not in the RSC in 3-month-old 5xFAD mice (Figure S4). Applying customized Sholl analysis (Figure 1c), we were able to monitor the spatial organization of the microglia processes between frames, as indicated by the color map plots (Figure 1d). Two-way ANOVA of microglia complexity, which was determined by the mean number of intersections between a single cell process and a standard set of spheres of gradually increasing diameter, did not detect an effect of the 5xFAD transgene ( $p = .255$ ) or ChABC treatment ( $p = 0.646$ ) or an interaction between these two factors ( $p = 0.417$ ) 24 hr after ChABC injection (Figure 1e). On day 3 (72 hr), imaging did not reveal a difference in the mean intersection number of the surveilling microglia processes between either the control and 5xFAD mice ( $p = .585$ ) or between the ChABC- and vehicle-treated mice ( $p = .842$ ); additionally, no interaction between treatment and genotype was detected ( $p = .679$ ; Figure 1e bottom). Three-way ANOVA of microglial complexity on Day 1 and Day 3 within each of the four groups revealed a significant decrease on Day 3 ( $p = .0449$ ); however, no effects of the other factors and no interaction between the time after injection and the other factors were detected ( $p > .05$ ).

For the same set of cells, we additionally measured the cell size and motility parameters to characterize the microglia under healthy and pathological conditions. The mean ramification distance, a parameter describing the microglial size, was not significantly affected by AD genotype ( $p = .112$ , two-way ANOVA) or ChABC treatment ( $p = .261$ ) at 24 hr or during chronic imaging at the 72 h time point ( $p = .380$  and  $p = .980$ , respectively). There was also no interaction between genotype and treatment 24 hr ( $p = .436$ ) or 72 hr ( $p = .557$ ) after ChABC injection.

Next, we estimated the motility index of single microglial cells by analyzing the change in the number of intersections as a function of the distance from the cell soma over time. AD genotype did not affect the motility index at 24 hr ( $p = .417$ ) or 72 hr ( $p = .605$ ). Additionally, treatment with ChABC had no effect ( $p = .530$  for the 24 hr time point and  $p = .847$  for the 72 hr time point), and there was no

interaction between treatment and genotype at 24 hr ( $p = .655$ ) or 72 hr ( $p = .734$ , two-way ANOVA, Figure 1g).

In summary, this data set demonstrates no significant differences in microglial size, complexity, or motility between the control and AD mice in the early age stages of pathology. Also, no effects of ChABC were detected on these parameters. In one out of the three parameters (the mean intersection number), we observed significantly decreased levels at 72 hr compared to 24 hr by three-way ANOVA.

### 3.3 | Microglial kinetics in acute response to single-cell damage is not affected by attenuation of ECM and amyloidosis

Given the perpetuating pro-inflammatory activation and progressive malfunction of microglial cells at advanced stages of AD (Keren-Shaul et al., 2017; Song et al., 2017), we have tried to clarify how the microglial response to damage is modified at the early stage. For this purpose, we have established a highly reproducible and controllable single microglial cell laser-induced focal ablation (SMCLA) method (Video S2; Davalos et al., 2005). As described above, we used customized Sholl analysis to perform a quantitative evaluation of the number of microglial processes reacting to the damage (Figure 2a) and to measure the velocity of the extension of the processes toward the lesion site. Our imaging analysis of the number of microglial processes approaching the site of the lesion revealed no significant effect of genotype ( $p = .765$ ) or treatment ( $p = .766$ ) on the mean intersection number at either the 24 hr time point or after 72 hr of chronic imaging after treatment ( $p = .673$  and  $p = .938$ , respectively, two-way ANOVA, Figure 2b). No interaction between both factors was observed ( $p = .153$  at 24 hr and  $p = .545$  at 72 hr). The induction of SMCLA *in vivo* produced a relatively equal number of microglial processes approaching the site of the lesion in all groups (Figure S5).

Next, we determined the velocity of the microglial processes approaching the microlesion site in the mice injected with ChABC and vehicle. There was no main effect of treatment ( $p = .105$ ) or AD genotype ( $p = .263$ ) 24 hr after injection or at the 72 hr time point ( $p = .562$  and  $p = .786$ , respectively, two-way ANOVA, Figure 3b). No interaction between treatment with ChABC and genotype (5xFAD) was detected ( $p = .103$  at 24 hr and  $p = .425$  at 72 hr). Together, these data suggest that the early phase of amyloidosis is not detrimental to the microglial process extension in response to SMCLA.

### 3.4 | Microglial cell migration is impaired by amyloidosis and rescued by attenuation of ECM

Next, we studied the effects of SMCLA with regard to the recruitment of microglial cell somas to the area of damage. According to our observations from pilot experiments, we expected relatively slow (from hours to days) microglial cell soma movements. Our evaluation



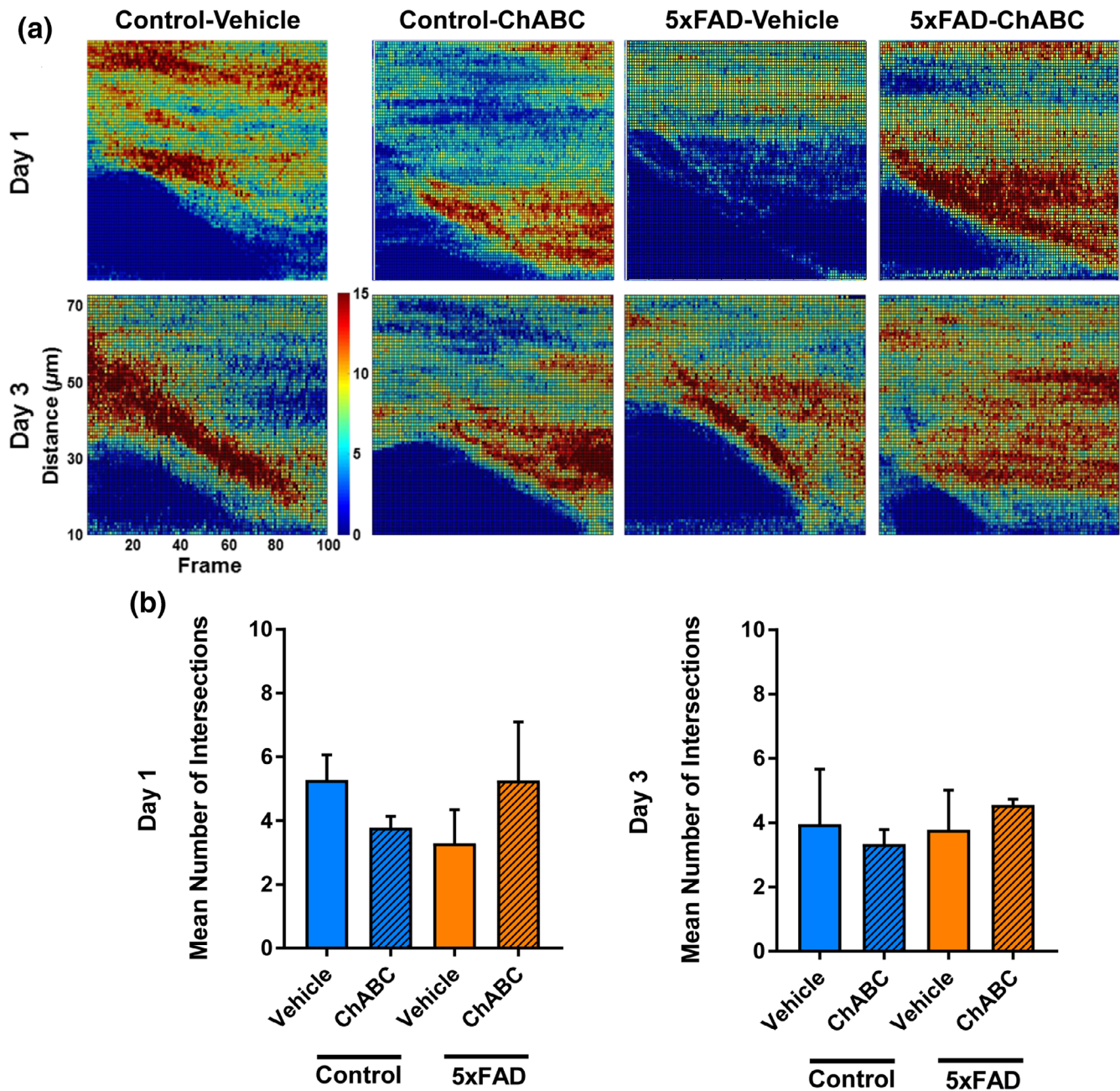


**FIGURE 2** Microglial acute response to damage in vivo is not modulated by ChABC and in 5xFAD mice. (a) Color maps of total microglia cell processes extension toward the lesion during recording in vivo. (b) Mean of total intersection number response to damage as a function of distance in Sholl analysis after vehicle or ChABC treatment. No difference between groups was detected at Day 1 and Day 3 by two-way ANOVA ( $n = 4/5$  mice, mean  $\pm$  SEM values are shown) [Color figure can be viewed at [wileyonlinelibrary.com](http://wileyonlinelibrary.com)]

focused on the recruitment of microglial cells to two circular areas: the central area of the damage (with a diameter of 125  $\mu\text{m}$ ) and the area surrounding the damage (with a diameter of 250  $\mu\text{m}$ ). We performed double-blinded quantification (see the materials and methods section for the criteria) of the number of microglial cells before induction of damage (Day 1) and 24 hr (Day 2), and 48 hr (Day 3) after the induction of damage. In response to SMCLA, the number of microglia in the central area was not affected by genotype ( $p = .533$ ) or treatment ( $p = .414$ ) on Day 2, but an interaction between genotype and treatment ( $p = .07$ , two-way ANOVA, Figure 4b) was revealed. On

Day 3, we observed no main effect of ChABC treatment ( $p = .459$ ) but did observe a trend for the effect of genotype ( $p = .072$ ) and a highly significant interaction ( $p = .002$ ) between treatment and genotype (5xFAD); ChABC reduced the number of recruited cells in the control mice but promoted microglia migration in the 5xFAD mice. Three-way ANOVA detected significant changes in the number of microglia during 3 days ( $p < .001$ ). The interaction of the three factors (treatment, genotype, and time) was significant ( $p = .001$ ; Figure 4b). These data are in line with the additional analysis of the number of microglial cells within the peripheral area surrounding the damaged



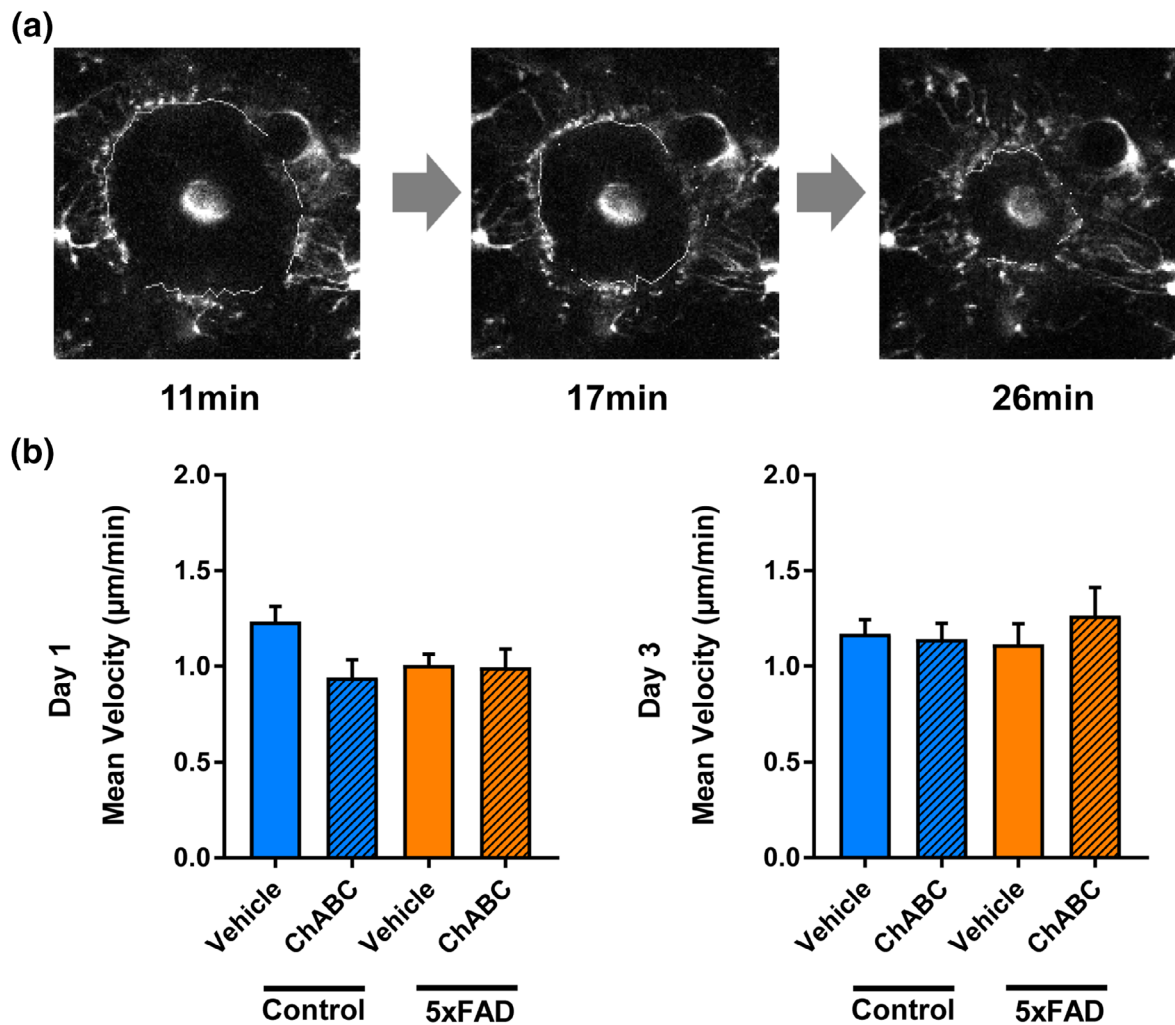


**FIGURE 3** Microglia process velocity in response to damage in vivo is not changed by ChABC treatment or in 5xFAD mice. (a) Microglia motility toward lesion in time-lapse in vivo. The lesion and microglia ROI consists of cell processes forming a circular shape (in white) with decreasing diameter toward the center in time. (b) The average velocity of microglia response in control and 5xFAD mice after the vehicle and ChABC treatments on Day 1 and Day 3. No difference between groups was detected by two-way ANOVA ( $n = 4/5$  mice, mean  $\pm$  SEM values are shown) [Color figure can be viewed at [wileyonlinelibrary.com](https://onlinelibrary.wiley.com/terms-and-conditions)]

site on Day 3, which also detected an interaction between genotype and treatment ( $p = .01$ , two-way ANOVA, Figure 5c), thus implying the importance of the microglia-ECM interaction for microglial migration/proliferation dynamics at the damage site.

In summary, we conclude that ChABC treatment promoted microglial cell recruitment to the lesion site on Day 3 (48 hr after damage) in 5xFAD mice but reduced migration in control animals. These data suggest a condition-dependent interaction between ECM components and microglia.

### 3.5 | Analysis of ECM and microglia migration-related gene expression in 5xFAD mice

The detected changes in microglia migration in 5xFAD mice might be related to (a) increase in expression of repellent ECM proteins or related

glycosyltransferases, resulting in a shift of expression of 4-sulfated versus 6-sulfated chondroitin sulfates; (b) decrease in expression of proteases cleaving these repellent ECM molecules; (c) decrease in expression of adhesive ECM and cell adhesion molecules stimulating microglia migration; (d) increase in expression of proteases cleaving such molecules. In an attempt to dissect between these mechanisms, we compared the expression of several candidate genes by quantitative RT-PCR in 4-month-old 5xFAD and control mice. The molecules of interest included CSPGs of the lectican family (ACAN, VCAN, NCAN, and BCAN) and phosphacan (PCAN/RPTPz1), enzymes involved in the synthesis of chondroitin sulfates (CHSY1 and 3; CHDP2; SHST3, 7, 11, 12, and 13) and hyaluronic acid (HAS1-3), link proteins (HAPLN1 and 4), tenascin-R (TNR) and -C (TNC), major heparan sulfate proteoglycans (glypicans 1, 2, and 4; syndecans 1 and 2; agrin), enzymes important for the synthesis of heparan sulfates (HS2ST1, HS3ST1, 3a and 5, HS6ST1 and 2), matrix metalloproteinases (MMP2, 9, 12 and 14;

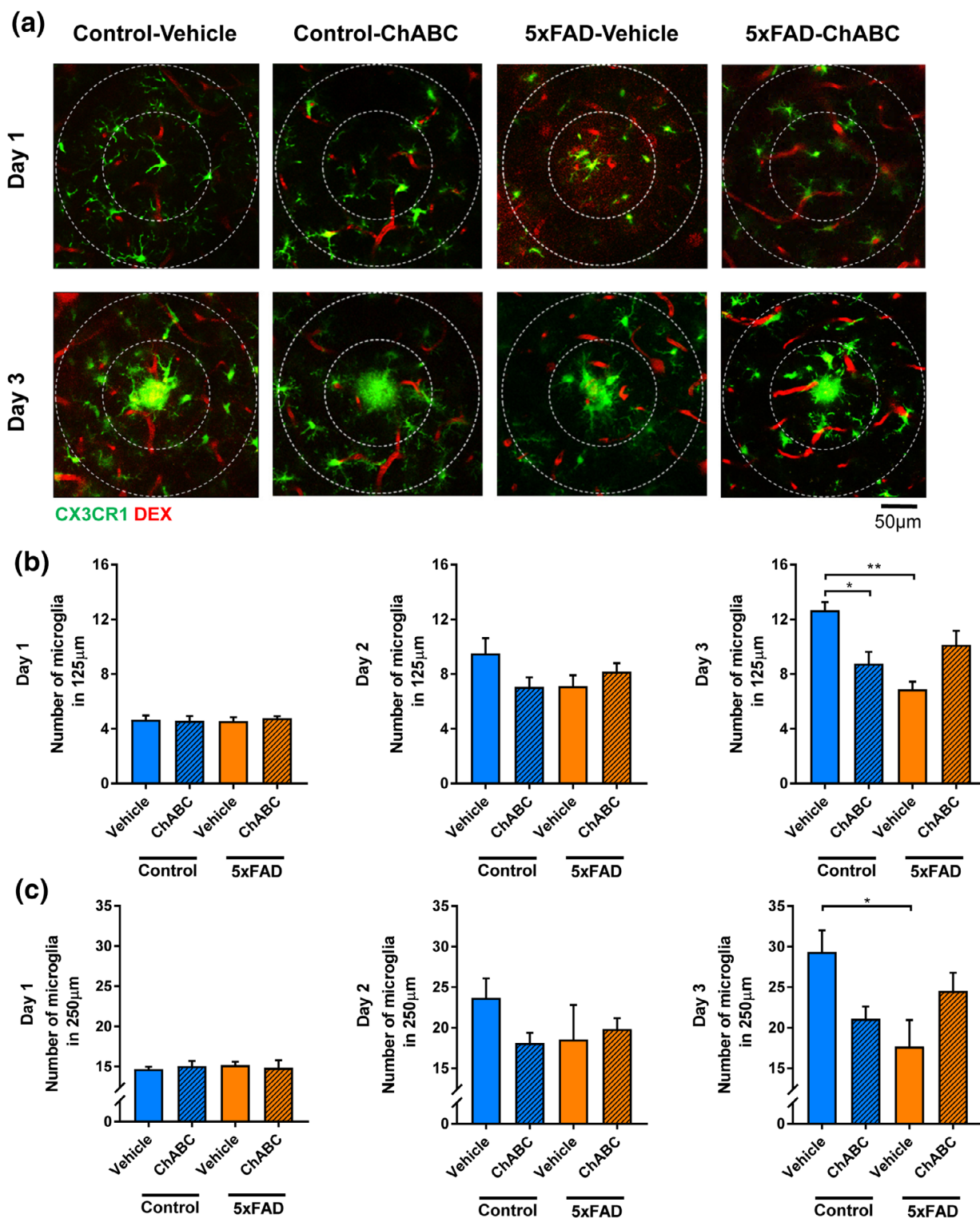


**FIGURE 4** Microglia cells recruitment in response to damage in vivo is impaired in 5xFAD mice. (a) The upper panel shows cell content in the center and extended area at 0 hr (Day1) before damage in vivo. The bottom panel shows the recruitment of cells in the photodamage site after 48 hr (Day3). (b) The mean number of microglial cells in the central ROI (diameter of 125  $\mu$ m). (c) The mean number of microglial cells in the extended ROI (diameter of 250  $\mu$ m). Differences between groups were analyzed by two-way ANOVA with *post hoc* Student–Newman–Keuls test (\* $p < .05$ , \*\* $p < .01$ ,  $n = 4/5$  mice, mean  $\pm$  SEM values are shown) [Color figure can be viewed at [wileyonlinelibrary.com](https://onlinelibrary.wiley.com/terms-and-conditions)]

ADAMTS4, 5, and 8), and their tissue inhibitors (TIMP1-3). Considering previously published genomics data (Landel et al., 2014) on genes dysregulated in 4-month-old 5xFAD mice, which have GO

terms related to migration and microglia, we also included heparinase (HPSE), protein tyrosine phosphatase receptor type C (PTPRC), cathepsin S (STSS), serpin family F member 2 (SERPINf2), collagen

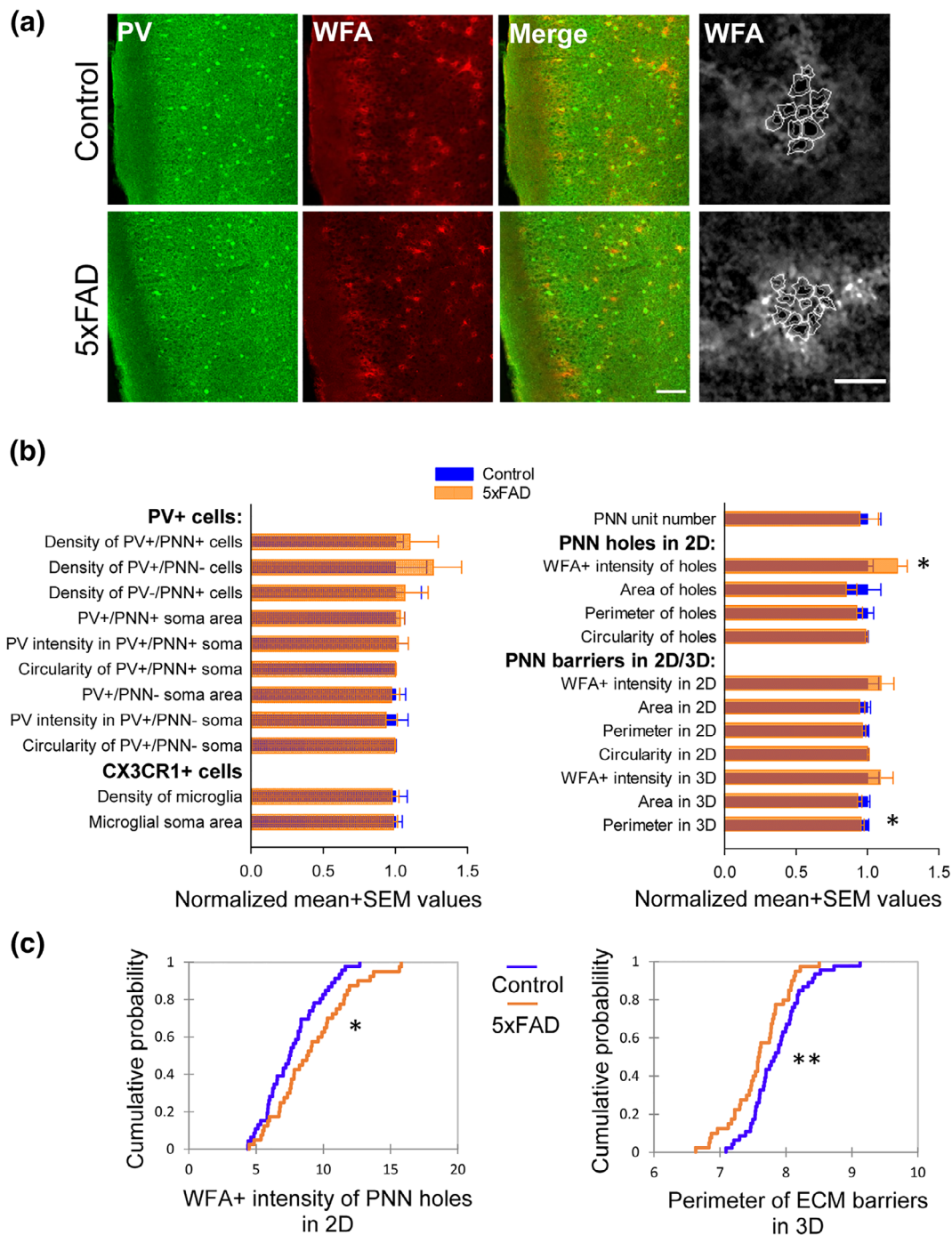


**FIGURE 5** Abnormalities in the fine structure of perineuronal nets in 5xFAD mice. (a) Histochemical analysis of PV and WFA expression in the RSC of 5xFAD and control mice. The right panels show high-resolution images of PNNs with traced holes (grey) and ECM barriers (white). Scale bars, 100 and 5  $\mu$ m. (b) Comparison of morphometric parameters characterizing PV+ interneurons, CX3CR1+ microglia, PNN holes and WFA+ ECM barriers. \* $p$  < .05, t-test.  $n$  = 6 mice. The values are normalized by the mean value in the control group. (c) Cumulative probability functions showing a higher intensity of WFA labeling in holes and smaller perimeter of ECM barriers in 5xFAD mice.  $n$  = 46 and 41 PNNs in control and 5xFAD mice, respectively. \* $p$  < .05 and \*\* $p$  < .01, the difference between genotypes, two-way ANOVA with animals as a nesting factor [Color figure can be viewed at [wileyonlinelibrary.com](http://wileyonlinelibrary.com)]

COL16a1, triggering receptor expressed on myeloid cells 2 (TREM2), microglial integrins (ITGAM, ITGAX, and ITGB2), CD36, and toll-like receptor 2 (TLR2) and TLR4 (Haage et al., 2019).

First, we confirmed the expression of human *App* and *Psn1* transgenes in the RSC, which proved to be higher than the expression of

corresponding endogenous mouse genes (Figure S6a). To evaluate possible dysregulation of multiple ECM and migration-related genes, we initially performed a primary screen using samples containing the whole cortex except for the RSC (Figure S6a–c). Dissected RSC samples were smaller and used in the secondary screen for the most interesting genes



and *Mmp12*, which turned out to be the only significantly upregulated gene in the primary screen. *Mmp12* upregulation was quite interesting as MMP12 may cleave fibronectin used as a substrate for cell migration. Chondroitinase ABC was reported to increase fibronectin expression (Lee et al., 2012), which would explain its normalizing effect in 5xFAD mice. However, analysis of MMP12 expression in RSC revealed no significant changes (Figure S6d). Other candidate genes involved in ECM remodeling and migration were also not significantly dysregulated (Figure S6d), although there was a tendency for upregulation of microglial integrin CD11c ( $p = .061$ ,  $t$ -test). In line with the absence of detectable A $\beta$  plaques, we did not detect increases in glial markers GFAP and IBA1 in the RSC.

Also, the immunohistochemical analysis of RSC did not reveal alterations in the number and size (related to activation) of microglial cells (Figure 5b). Similarly, the number and size of parvalbumin (PV)+ interneurons and PNNs, associated and nonassociated with PV+ interneurons were not affected in 5xFAD mice (Figure 5a,b). However, more detailed analysis of parameters characterizing the fine structure of PNNs, that is, the intensity of WFA labeling, the size and shape of holes and ECM barriers around them (Figure 5a), revealed an increase in the intensity of WFA labeling in holes and a reduction in the perimeter of ECM barriers in 5xFAD mice (Figure 5b,c). In summary, no major hallmarks of neuroinflammation and just subtle changes in the fine organization of neural ECM are detectable in the RSC of 4-month-old 5xFAD mice.

### 3.6 | Flow cytometric analysis of cell composition and activation after attenuation of ECM

Previously, we suggested that AD pathology in the brain parenchyma may be associated with the release of certain inflammatory mediators that cause the recruitment of innate immune cells to specific brain regions (Mohle, Israel, et al., 2016; Pannell et al., 2020). To ascertain the conditions of the early stages of AD and the pathophysiological relevance of ECM attenuation *in vivo*, we employed flow cytometric analysis to determine the activation of microglia and the recruitment of peripheral cells into the RSC in the control and 5xFAD mice. The brain tissue samples were analyzed at 72 hr after surgery and ChABC injection and cells were identified according to their expression of CD45 and CD11b as depicted in Figure 6a–c. When compared to that in the naïve control animals, the number of CD11b<sup>+</sup> cells in the animal groups that underwent surgery was significantly elevated in the mice treated with ChABC (control-naïve:  $58.23 \pm 4.36\%$ , control-vehicle:  $67.23 \pm 7.34\%$ , control-ChABC:  $81.27 \pm 4.96\%$ ). The naïve 5xFAD mice did not show a difference in CD11b<sup>+</sup> cell number compared to that in the naïve control mice; however, we found that, upon craniotomy, the percentage of CD11b<sup>+</sup> cells increased similarly for both the 5xFAD-vehicle and 5xFAD-ChABC animals (5xFAD-naïve:  $47.37 \pm 2.72\%$ , 5xFAD-vehicle:  $74.13 \pm 2.06\%$ , 5xFAD-ChABC:  $72.40 \pm 2.87\%$ ).

According to our strategy for cell-type determination (shown in Figure 6a–c), CD11b<sup>+</sup> cells were separated into either resident brain microglial cells or recruited peripheral myeloid cells. As expected, microglia represented the majority of the CD11b<sup>+</sup> cells in the naïve

control ( $98.70 \pm 0.29\%$ ) and 5xFAD mice ( $98.47 \pm 0.07\%$ ), whereas myeloid cells were only detected as a small fraction (control-naïve:  $0.63 \pm 0.08\%$ , 5xFAD-naïve:  $0.72 \pm 0.03\%$ ; Figure 6d,e). Two-way ANOVA revealed a significant effect of treatment ( $p < .0001$ ) and no effect of genotype ( $p = .219$ ) on the number of myeloid cells 72 hr after surgery, as well as an interaction between treatment and genotype ( $p = .031$ ). The proportion of myeloid cells increased significantly in both the control-vehicle ( $10.78 \pm 4.87\%$ ;  $p = .021$ , two-way ANOVA) and control-ChABC groups ( $14.93 \pm 2.24\%$ ;  $p = .006$ ) (Figure 6e). In the brains of the 5xFAD mice injected with vehicle, we detected an even stronger increase in myeloid cells ( $20.73 \pm 1.39\%$ ,  $p < .001$ ) compared to that in the controls. However, compared to vehicle injection, the administration of ChABC was associated with a reduced influx of recruited peripheral cells ( $11.28 \pm 1.40\%$ ,  $p = .033$ ) in the 5xFAD mice. Opposite changes were observed in the percentage of microglial cells (Figure 6d).

Furthermore, we analyzed the effects of ChABC administration on the activation status of resident microglia in the RSC (Figure 6f–i).

The expression levels of microglial surface markers were assessed by flow cytometric analysis of the MFI. Resident microglia express low levels of the leukocyte common antigen CD45 in the resting stage, and upon exposure to inflammatory stimuli, activated microglia upregulate the expression of CD45 (Ginhoux et al., 2010; Rice et al., 2017). Two-way ANOVA revealed a highly significant effect of treatment ( $p < .0001$ ) on the expression of CD45, and an interaction between treatment and genotype ( $p = .011$ ). When compared to the naïve control mice, the mice injected with either vehicle or ChABC displayed a significant increase in microglial CD45 expression (control-naïve:  $5265 \pm 196.6$  vs. control-vehicle:  $7175 \pm 415$ ,  $p = .001$ ; control-naïve vs. control-ChABC:  $8386 \pm 440.1$ ,  $p < .0001$ ; Figure 6f). Corresponding to these findings, microglia in the 5xFAD mice also exhibited an upregulated surface expression level of CD45 after surgery (5xFAD-naïve:  $5301 \pm 110.2$  vs. 5xFAD-vehicle:  $7946 \pm 77.23$ ,  $p < .0001$ ), and the detected MFIs did not differ from that of the control mice. The 5xFAD-ChABC mice exhibited reduced activation of microglia ( $7232 \pm 37.9$ ) compared to that in the control-ChABC ( $p = .024$ ) and 5xFAD-vehicle ( $p = .08$ ) groups.

Another marker used to determine microglial activity is the major histocompatibility complex (MHC) class I molecule, which also becomes upregulated upon injury-induced cell activation (Moffett & Paden, 1994; Tooyama, Kimura, Akiyama, & McGeer, 1990; Figure 6g). Two-way ANOVA detected no effect of genotype ( $p = .563$ ), a trend for interaction between genotype and treatment ( $p = .098$ ), and a strong effect of treatment ( $p < .001$ ) on the expression of MHC I. This effect was similar to that described for CD45: the mice injected with either vehicle or ChABC showed significantly higher expression of MHC I (one-way ANOVA,  $p < .0001$ ; Figure 6g) than that of the control-naïve mice (naïve:  $945.7 \pm 23.38$ , vehicle:  $1310 \pm 164.3$ , ChABC:  $1643 \pm 111.9$ ) and the 5xFAD-naïve mice (naïve:  $956 \pm 26.46$ , vehicle:  $1576 \pm 18.98$ , ChABC:  $1495 \pm 71.3$ ).

The surface molecule CD11c, known as the transmembrane protein integrin alpha X (ITGAX), is present on dendritic cells and macrophages (Figure 6h). The expression level of CD11c is associated with the activation level of antigen-presenting cells (Kettenmann, Hanisch, Noda, &



Verkhatsky, 2011; Remington, Babcock, Zehntner, & Owens, 2007). There was no effect of genotype ( $p = .915$ ), treatment ( $p = .1$ ), or interaction between genotype and treatment ( $p = .931$ ). The MFI values of CD11c in the control (naïve:  $323 \pm 26.46$ , vehicle:  $439.3 \pm 78.12$ , ChABC:  $394.3 \pm 21.85$ ) and 5xFAD mice (naïve:  $343.7 \pm 38.67$ , vehicle:  $427.7 \pm 29.38$ , ChABC:  $396.7 \pm 35.79$ ) were similar.

Furthermore, we used flow cytometry to analyze the expression levels of  $\beta 1$ -integrin (CD29), which is thought to be involved in microglial activation and migration in neurodegenerative diseases (Kim et al., 2014; Figure 6i). Two-way ANOVA detected no effect of genotype ( $p = .269$ ) and no interaction between genotype and treatment on the expression of CD29 ( $p = .981$ ) but revealed an effect of

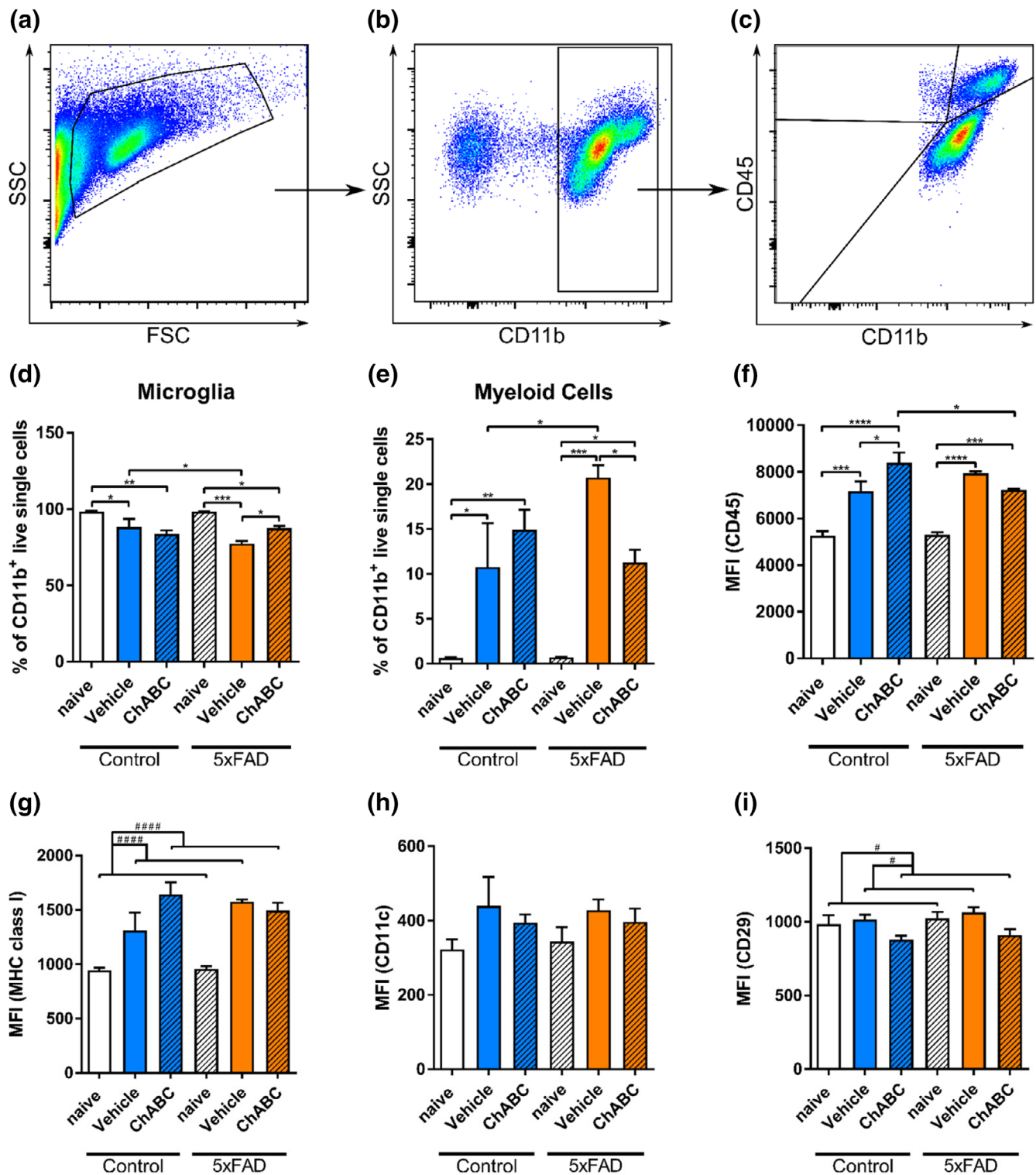


**FIGURE 6** Legend on next page.

treatment ( $p = .012$ ). Microglial CD29 surface expression was significantly lower in ChABC-treated mice than in the naïve or vehicle-treated animals (one-way ANOVA,  $p < .05$ ), independent of genotype (control-naïve:  $983.3 \pm 61.78$ , control-vehicle:  $1016 \pm 32.76$ , control-ChABC:  $878.3 \pm 27.29$ ; 5xFAD-naïve:  $10236 \pm 45.11$ , 5xFAD-vehicle:  $1064 \pm 35.02$ , 5xFAD-ChABC:  $909 \pm 40.51$ ).

In conclusion, 72 hr after craniotomy, 5xFAD-vehicle mice showed increased recruitment of myeloid cells compared to that in the control-vehicle mice. Strikingly, ChABC administration increased recruitment in the control but reduced recruitment in 5xFAD mice. Furthermore, ChABC treatment also resulted in an attenuated activation of microglia in the 5xFAD, which was in contrast to our findings in the control group. Finally, in line with the two-photon imaging data, we showed that, in the control and 5xFAD animals, the administration of ChABC did not affect microglia complexity or dendritic functionality, as represented by the surface expression levels of CD29 and CD11c, respectively.

## 4 | DISCUSSION

In this study, we focused on the RSC as a region that is affected early in patients with AD pathology (Dillen et al., 2017; Pai & Yang, 2013; Tan, Wong, Hodges, Halliday, & Hornberger, 2013). We aimed to investigate the functional deficits of microglial cells in the RSC at the stage preceding the accumulation of amyloid plaques in this region (3–4 months of age) in a widely used mouse model of amyloidosis/AD. It remains unclear whether microglial impairment in the early phase of amyloidosis can contribute to pathogenesis. Using ChABC to attenuate the neural ECM in vivo, we were able to measure microglial dynamics by two-photon microscopy in CX3CR1<sup>gfp+/-</sup> x 5xFAD. BL6<sup>-/-</sup> mice in vivo. Our findings suggest a model in which the microglia-ECM interaction is essential to control the kinetics of microglial recruitment to a damage site and thus might provide a framework for a better understanding of the early stages of neurodegeneration.

First, we determined the basal levels of microglial complexity, motility and size. Our two-photon recordings on Days 1 and 3 after surgery showed no deficits in the microglia motility index, microglial complexity, or microglial size in the 5xFAD mice after in vivo treatment with vehicle or ChABC. To our knowledge, this is the first direct comparison of healthy and amyloidosis-affected microglia in the early

stages of pathology. Our data are consistent with other studies showing impairment in the baseline dynamics of plaque-associated microglia but not in the pathology-free parenchyma (Bolmont et al., 2008; Koenigsnecht-Talboo et al., 2008; Krabbe et al., 2013). Furthermore, a study by Bolmont et al. (2008) in APP/PS1 transgenic mice detected no difference in the microglial process extension-retraction rate near A $\beta$  plaques, but this rate was impaired in “on-plaque” microglia. To our knowledge, we are the first to assess the total number of microglial processes advancing toward an acute injury induced by laser ablation of a single cell in young 5xFAD mice in vivo. The microglial response in the RSC of 5xFAD mice in the early stage of amyloidosis was not changed compared to that in healthy controls. Notably, another group reported dysfunctional microglial process extension in an aged APP/PS1 mouse model of AD with an accelerated burden of A $\beta$  plaques (Krabbe et al., 2013). Hence, the combination of the evidence from this previous study and our present data point to the plaque-dependent/soluble A $\beta$ -independent regulation of microglial shape during the advanced stages of AD.

As another approach, we determined microglial function in vivo by counting the number of microglial cells recruited to the site of damage after 24 and 48 hr. Our approach revealed a significantly reduced number of recruited microglia cells in the RSC of the 5xFAD mice after damage at the 48 hr time point on Day 3 postsurgery. Thus, our data may link the early stage pathology-associated functional impairment in microglial migration in 3- to 4-month-old AD model mice. The putative mechanisms of this failure are still not clear, but there are several hypotheses. First, microglia polarization to the pro-inflammatory phenotype (due to surgery in our case) may contribute significantly to changes in microglial migration, as was shown by other colleagues (Gao et al., 2019; Garden & Campbell, 2016; Landel et al., 2014), who measured several molecular markers involved in inflammation and immunomodulation. The expression of *Clec7a* (which codes for the dectin-1 protein), *Cst7* (cystatin F), *Itgax* (CD11c), and genes encoding the chemokines *Ccl3*, *Ccl4*, *Ccl6*, and glial fibrillary acidic protein (GFAP) turned out to be increased in the cortex of 5xFAD mice. Another possible mechanism is the decreasing levels of sulfatide in the cortex of 3-month-old 5xFAD mice that have been observed by Hong et al., 2016 (Hong et al., 2016). Sulfatide is a major lipid component of the myelin sheath that has recently been implicated in neurodegeneration through the induction of pathological inflammatory responses in microglia (Jeon, Yoon, Park, Kim, & Park, 2008). Additionally, we speculate that the modification of ECM

**FIGURE 6** Flow cytometric analysis of immune cells isolated from RBC naïve and treated control and 5xFAD mice. (a–c) Plots display the representative strategy for cell type discrimination utilized to identify immune cell populations. After selection of cellular events in the forward-scatter/side-scatter plot (FSC/SSC), dead cells were excluded and only single-cell events were used for further analysis (not shown). (b) Next, only cells positively expressing the CD11b surface marker were selected. (c) Subsequently, these cells were divided according to their expression of CD45 and CD11b into brain resident microglia (CD45<sup>int</sup>CD11b<sup>int</sup>, lower right gate) and infiltrated peripheral myeloid cells (CD45<sup>hi</sup>CD11b<sup>hi</sup>, upper right gate). (d,e) Bar charts show the frequencies of identified cell populations. Cells were selected as described above and bars display the population as percent of living single CD11b positive events. (f,g) Flow cytometric analysis of surface marker expression level on isolated microglial cells. Bar charts display the median fluorescence intensity (MFI) of the corresponding fluorescence-conjugated antibody. Differences between groups were analyzed by two-way ANOVA, followed by one-way ANOVA ( $^{\#}p < .05$ ,  $^{####}p < .0001$ ) or *post hoc* Student–Newman–Keuls test ( $^{*}p < .05$ ,  $^{**}p < .01$ ,  $^{***}p < .001$ ,  $^{****}p < .0001$ ,  $n = 3$  mice per group, mean  $\pm$  SEM values are shown) [Color figure can be viewed at [wileyonlinelibrary.com](http://wileyonlinelibrary.com)]



in AD may be responsible for the impaired microglial migration. Indeed, the following observations support the latter hypothesis. Although we could not detect any major changes in gene expression of ECM molecules and related enzymes responsible for posttranslational modification of ECM molecules, we found alterations in the fine ECM organization of PNNs, which is a condensed form of neural ECM similar to widespread form of interstitial perisynaptic ECM in the neuropil. The attenuation of the ECM by ChABC *in vivo* restored microglial recruitment to the RSC of 5xFAD mice on Day 2 after injury with an even stronger effect on Day 3. This effect was observed in the SMCLA paradigm in the central part of the damage as well as in the surrounding periphery. Thus, we suggest that the microglial activation phenotype is time-dependent, with the most prominent effects of ChABC treatment occurring on Day 3 after surgery and injection. It appears that ECM digestion counteracts the mechanisms activated by amyloidosis with respect to the surgical activation of microglia. Several pathways may be involved; mechanically, microglial processes are closely intertwined with dynamic synaptic junctions, and this, as has been shown previously, may inhibit fine motility. It has been previously reported that treatment with ChABC *in vivo* successfully degrades inhibitory proteoglycan substrates and thereby promotes further axon sprouting and regeneration (Bradbury et al., 2002; Steinmetz et al., 2005). A combination of ChABC and cell culture media conditioned by alternatively activated macrophages stronger promoted axonal growth across an inhibitory CSPG gradient than ChABC combined with the media conditioned by classically activated macrophages (Kigerl et al., 2009). Indeed, ChABC treatment alters the expression of several genes characteristic of activated macrophages. It elevates expression of anti-inflammatory cytokine IL-10 and decreases expression of pro-inflammatory cytokine IL-12 $\beta$  (Mantovani, Biswas, Galdiero, Sica, & Locati, 2013), and upregulates CD206, CD16, ARG1, and CD32 (Kigerl et al., 2009). The administration of ChABC in the spinal cord results in the upregulation of IBA1 expression by macrophages and microglia, as well as of the leukocyte common antigen CD45 (Didangelos et al., 2014). These findings are in line with our observations of not only decreased response to damage in control mice 3 days after treatment with ChABC, but also the impairment of microglial cell recruitment to the site of the damage after 24 hr. This overall trend of declining functional capacity in the control ChABC-treated mice is strikingly different from the effects observed in the 5xFAD ChABC-treated mice. Similarly, ChABC treatment impairs LTP in wild-type mice (Bukalo, Schachner, & Dityatev, 2001), but restores LTP in 5xFAD mice and in models of tauopathy (Yang et al., 2015).

Finally, we determined the effect of *in vivo* ChABC treatment on the expression of markers of microglial activation in the RSC by flow cytometry. For that purpose, we used well-established CD11b and CD45 antibodies, which helped to reliably identify not only resident microglia cells, but also recruited myeloid cells. The number of myeloid cells varied; for instance, in the 5xFAD-vehicle mice, it reached 21% of the overall population of labeled cells, which was twice as high as in that in the control-vehicle and 5xFAD-ChABC groups. Our results suggest that myeloid cell infiltration mechanisms may be

affected in the early stage of AD and are partially under the control of the ECM. Our data are thus complementary to a number of genetic studies (Jay et al., 2015; Wang et al., 2015) that focused on TREM2 expression on myeloid cells and microglia in amyloid pathology.

Our finding of increased CD45 expression in the RSC of control-ChABC but not 5xFAD-ChABC mice is in line with the aforementioned genotype-specific effect of ChABC on microglial behavior. However, the injected groups displayed a significant elevation of CD45 expression compared to that in the naïve untreated animals, which implicates the effects of surgery on these conditions. CD45 has been associated with Alzheimer's pathology by the work of Zhu and colleagues (Zhu et al., 2011), which described a positive correlation between CD45 and A $\beta$  deposition in PSAPP/CD45<sup>-/-</sup> mice. It is plausible to assume that ChABC treatment may modulate the levels of A $\beta$  depositions and thus counteract amyloidosis during specific windows of time after injection; however, more studies are needed to address this question experimentally. The expression of MHC class I was also elevated after the injection of vehicle or ChABC compared to the levels observed in both the control naïve and 5xFAD naïve mice. Similar to the effects on CD45 expression, ChABC treatment tended to elevate the levels of MHC class I in the control-ChABC group but not in the 5xFAD mice, although this effect was less prominent than that on CD45 expression. These data imply a very specific role for ChABC-digested ECM glycans and their associated molecules in the regulation of the microglial immune response *in vivo*.

We expected CD11c to be particularly elevated in AD (Raj et al., 2017), but in our samples, the naïve young 5xFAD mice displayed no increase in basal control conditions. These data are consistent with comparisons between the 5xFAD-vehicle mice that underwent surgery and age-matched controls. Furthermore, treatment with ChABC had no effect on either the control or 5xFAD mice. This result contradicts the still unconfirmed hypothesis that the increased expression of immune factors underlies AD-like pathology in the early stages (Krstic et al., 2012). Another marker we tested is CD29, a protein involved in the ramification of microglia. ChABC treatment slightly but significantly reduced CD29 expression in both the control and 5xFAD mice, which may imply a putative role of the ECM in the regulation of immunoglobulin expression in microglia.

Finally, published data indicate that A $\beta$  oligomers may provide signals controlling the migration of microglial cells (Zhong et al., 2018). We hypothesize that these widely spread signals in 5xFAD mice may mask/override the focal signal generated after cell photoablation and hence, impair directed migration to the side of the lesion. RhoA/ROCK signaling has been implicated in A $\beta$ -induced responses of microglial cells (Zhang et al., 2019). As ChABC treatment may abrogate activation of RhoA-ROCK pathway by chondroitin sulfates via PTP $\sigma$  (Pendleton et al., 2013) and reduce expression of RhoA (Day, Alves, Daniell, Dasgupta, & Ogborne, 2020), we shall further investigate the relevance of this pathway in early microglia migration defects in AD mouse models and patients.

To date, the systematic evaluation of the ECM in neuroinflammation has received insufficient attention. With the progression of A $\beta$  plaque pathology and the worsening of clinical dementia

symptoms, microglial activation becomes an indirect measure of damage. Here, we provide evidence for early-stage defects in microglia-induced neuroinflammation in the RSC of young AD model mice. This observation may be related to the disrupted hippocampus/default mode network connection in prodromal AD patients (Dillen et al., 2017). Hence, compromised connectivity throughout the RSC may be correlated to a certain degree with impaired microglial cell function. Under these conditions, the microglia phenotype was at least partly normalized due to the attenuation of the ECM. However, further studies are needed to address and elucidate the underlying molecular mechanisms. Considering the emerging options for positron emission tomography imaging of microglia in humans (Horti et al., 2019), it might be possible to estimate the efficacy of microglia migration to sites of vascular microdamage or focal transcranial stimulation and use such measures as early biomarkers of AD (Han, Zhu, & Zhang, 2019).

## ACKNOWLEDGMENTS

We thank the China Scholarship Council for the State Scholarship Fund awarded to Weilun Sun (grant number 201406170032). This study was supported by the federal state Saxony-Anhalt and the European Structural and Investment Funds (ESF, 2014–2020), project number ZS/2016/08/80645 (to Alexander Dityatev), and Deutsche Forschungsgemeinschaft (GRK SynAge 2413/1, TP5 to Ildiko Rita Dunay and TP6 to Alexander Dityatev). Open access funding enabled and organized by Projekt DEAL.

## CONFLICT OF INTEREST

The authors declare no competing financial interests.

## DATA AVAILABILITY STATEMENT

The data that support the findings of this study are available from the corresponding author upon reasonable request.

## ORCID

Stoyan Stoyanov  <https://orcid.org/0000-0002-2872-7709>

Weilun Sun  <https://orcid.org/0000-0001-6374-1277>

Henning Peter Düsedau  <https://orcid.org/0000-0002-0805-4084>

Carla Cangalaya  <https://orcid.org/0000-0002-3525-8445>

David Baidoe-Ansah  <https://orcid.org/0000-0002-3787-9958>

Rahul Kaushik  <https://orcid.org/0000-0002-4944-8549>

Ildiko Rita Dunay  <https://orcid.org/0000-0002-9900-8605>

Alexander Dityatev  <https://orcid.org/0000-0002-0472-0553>

## REFERENCES

- Baidoe-Ansah, D., Sakib, S., Jia, S., Fischer, A., Kaushik, R., & Dityatev, A. (2019). Epigenetic mechanism of carbohydrate sulfotransferase 3 (CHST3) ownregulation in the aging brain. *bioRxiv*. <https://doi.org/10.1101/741355>
- Bartus, K., James, N. D., Didangelos, A., Bosch, K. D., Verhaagen, J., Yanez-Munoz, R. J., ... Bradbury, E. J. (2014). Large-scale chondroitin sulfate proteoglycan digestion with chondroitinase gene therapy leads to reduced pathology and modulates macrophage phenotype following spinal cord contusion injury. *The Journal of Neuroscience*, 34(14), 4822–4836. <https://doi.org/10.1523/jneurosci.4369-13.2014>
- Biswas, A., Bruder, D., Wolf, S. A., Jeron, A., Mack, M., Heimesaat, M. M., & Dunay, I. R. (2015). Ly6C(high) monocytes control cerebral toxoplasmosis. *Journal of Immunology*, 194(7), 3223–3235. <https://doi.org/10.4049/jimmunol.1402037>
- Biswas, A., French, T., Dusedau, H. P., Mueller, N., Riek-Burchardt, M., Dudeck, A., ... Dunay, I. R. (2017). Behavior of neutrophil granulocytes during toxoplasma gondii infection in the central nervous system. *Frontiers in Cellular and Infection Microbiology*, 7, 259. <https://doi.org/10.3389/fcimb.2017.00259>
- Bolmont, T., Haiss, F., Eicke, D., Radde, R., Mathis, C. A., Klunk, W. E., ... Calhoun, M. E. (2008). Dynamics of the microglial/amyloid interaction indicate a role in plaque maintenance. *The Journal of Neuroscience*, 28(16), 4283–4292. <https://doi.org/10.1523/jneurosci.4814-07.2008>
- Bradbury, E. J., Moon, L. D., Popat, R. J., King, V. R., Bennett, G. S., Patel, P. N., ... McMahon, S. B. (2002). Chondroitinase ABC promotes functional recovery after spinal cord injury. *Nature*, 416(6881), 636–640. <https://doi.org/10.1038/416636a>
- Bruckner, G., Bringmann, A., Hartig, W., Koppe, G., Delpech, B., & Brauer, K. (1998). Acute and long-lasting changes in extracellular-matrix chondroitin-sulphate proteoglycans induced by injection of chondroitinase ABC in the adult rat brain. *Experimental Brain Research*, 121(3), 300–310.
- Bukalo, O., Schachner, M., & Dityatev, A. (2001). Modification of extracellular matrix by enzymatic removal of chondroitin sulfate and by lack of tenascin-R differentially affects several forms of synaptic plasticity in the hippocampus. *Neuroscience*, 104(2), 359–369.
- Condello, C., Yuan, P., Schain, A., & Grutzendler, J. (2015). Microglia constitute a barrier that prevents neurotoxic protofibrillar Abeta42 hot-spots around plaques. *Nature Communications*, 6, 6176. <https://doi.org/10.1038/ncomms7176>
- Davalos, D., Grutzendler, J., Yang, G., Kim, J. V., Zuo, Y., Jung, S., ... Gan, W. B. (2005). ATP mediates rapid microglial response to local brain injury in vivo. *Nature Neuroscience*, 8(6), 752–758. <https://doi.org/10.1038/nn1472>
- Day, P., Alves, N., Daniell, E., Dasgupta, D., & Osborne, R. (2020). Targeting chondroitinase ABC to axons enhances the ability of chondroitinase to promote neurite outgrowth and sprouting. *PLoS One*, 15(1), e0221851. <https://doi.org/10.1371/journal.pone.0221851>
- Didangelos, A., Iberl, M., Vinsland, E., Bartus, K., & Bradbury, E. J. (2014). Regulation of IL-10 by chondroitinase ABC promotes a distinct immune response following spinal cord injury. *The Journal of Neuroscience*, 34(49), 16424–16432. <https://doi.org/10.1523/jneurosci.2927-14.2014>
- Dillen, K. N. H., Jacobs, H. I. L., Kukolja, J., Richter, N., von Reutern, B., Onur, O. A., ... Fink, G. R. (2017). Functional disintegration of the default mode network in prodromal Alzheimer's disease. *Journal of Alzheimer's Disease*, 59(1), 169–187. <https://doi.org/10.3233/jad-161120>
- Do Carmo, S., & Cuello, A. C. (2013). Modeling Alzheimer's disease in transgenic rats. *Molecular Neurodegeneration*, 8, 37. <https://doi.org/10.1186/1750-1326-8-37>
- Dusedau, H. P., Klevevan, J., Figueiredo, C. A., Biswas, A., Steffen, J., Kliche, S., ... Dunay, I. R. (2019). p75(NTR) regulates brain mononuclear cell function and neuronal structure in toxoplasma infection-induced neuroinflammation. *Glia*, 67(1), 193–211. <https://doi.org/10.1002/glia.23553>
- Farfara, D., Feierman, E., Richards, A., Revenko, A. S., MacLeod, R. A., Norris, E. H., & Strickland, S. (2019). Knockdown of circulating C1 inhibitor induces neurovascular impairment, glial cell activation, neuroinflammation, and behavioral deficits. *Glia*, 67(7), 1359–1373. <https://doi.org/10.1002/glia.23611>
- Fawcett, J. W., & Asher, R. A. (1999). The glial scar and central nervous system repair. *Brain Research Bulletin*, 49(6), 377–391.
- Figueiredo, C. A., Düsedau, H. P., Steffen, J., Gupta, N., Dunay, M. P., Toth, G. K., ... Dunay, I. R. (2019). Immunomodulatory effects of the neuropeptide pituitary adenylate cyclase-activating polypeptide in





- acute toxoplasmosis. *Frontiers in Cellular and Infection Microbiology*, 9, 154. <https://doi.org/10.3389/fcimb.2019.00154>
- Frisoni, G. B., Pievani, M., Testa, C., Sabatelli, F., Bresciani, L., Bonetti, M., ... Thompson, P. M. (2007). The topography of grey matter involvement in early and late onset Alzheimer's disease. *Brain*, 130(Pt 3), 720–730. <https://doi.org/10.1093/brain/awl377>
- Gao, T., Jernigan, J., Raza, S. A., Dammer, E. B., Xiao, H., Seyfried, N. T., ... Rangaraju, S. (2019). Transcriptional regulation of homeostatic and disease-associated-microglial genes by IRF1, LXR $\beta$ , and CEBP $\alpha$ . *Glia*, 67(10), 1958–1975. <https://doi.org/10.1002/glia.23678>
- Garden, G. A., & Campbell, B. M. (2016). Glial biomarkers in human central nervous system disease. *Glia*, 64(10), 1755–1771. <https://doi.org/10.1002/glia.22998>
- Ginhoux, F., Greter, M., Leboeuf, M., Nandi, S., See, P., Gokhan, S., ... Merad, M. (2010). Fate mapping analysis reveals that adult microglia derive from primitive macrophages. *Science*, 330(6005), 841–845. <https://doi.org/10.1126/science.1194637>
- Haage, V., Elmadany, N., Roll, L., Faissner, A., Gutmann, D. H., Semtner, M., & Kettenmann, H. (2019). Tenascin C regulates multiple microglial functions involving TLR4 signaling and HDAC1. *Glia*, 81, 470–483. <https://doi.org/10.1016/j.bbi.2019.06.047>
- Han, J., Zhu, K., & Zhang, X. M. (2019). Enforced microglial depletion and repopulation as a promising strategy for the treatment of neurological disorders. *Glia*, 67(2), 217–231. <https://doi.org/10.1002/glia.23529>
- Hartig, W., Derouiche, A., Welt, K., Brauer, K., Grosche, J., Mader, M., ... Bruckner, G. (1999). Cortical neurons immunoreactive for the potassium channel Kv3.1b subunit are predominantly surrounded by perineuronal nets presumed as a buffering system for cations. *Brain Research*, 842(1), 15–29.
- Heneka, M. T., Kummer, M. P., Stutz, A., Delekate, A., Schwartz, S., Vieira-Saecker, A., ... Golenbock, D. T. (2013). NLRP3 is activated in Alzheimer's disease and contributes to pathology in APP/PS1 mice. *Nature*, 493(7434), 674–678. <https://doi.org/10.1038/nature11729>
- Hofrichter, J., Krohn, M., Schumacher, T., Lange, C., Feistel, B., Walbroel, B., ... Pahnke, J. (2013). Reduced Alzheimer's disease pathology by St. John's Wort treatment is independent of hyperforin and facilitated by ABCC1 and microglia activation in mice. *Current Alzheimer Research*, 10(10), 1057–1069.
- Holtmaat, A., Bonhoeffer, T., Chow, D. K., Chuckowree, J., De Paola, V., Hofer, S. B., ... Wilbrecht, L. (2009). Long-term, high-resolution imaging in the mouse neocortex through a chronic cranial window. *Nature Protocols*, 4(8), 1128–1144. <https://doi.org/10.1038/nprot.2009.89>
- Hong, J. H., Kang, J. W., Kim, D. K., Baik, S. H., Kim, K. H., Shanta, S. R., ... Kim, K. P. (2016). Global changes of phospholipids identified by MALDI imaging mass spectrometry in a mouse model of Alzheimer's disease. *Journal of Lipid Research*, 57(1), 36–45. <https://doi.org/10.1194/jlr.M057869>
- Horti, A. G., Naik, R., Foss, C. A., Minn, I., Misheneva, V., Du, Y., ... Calabresi, P. A. (2019). PET imaging of microglia by targeting macrophage colony-stimulating factor 1 receptor (CSF1R). *Proceedings of the National Academy of Sciences of the United States of America*, 116(5), 1686–1691. <https://doi.org/10.1073/pnas.1812155116>
- Jay, T. R., Miller, C. M., Cheng, P. J., Graham, L. C., Bemiller, S., Broihier, M. L., ... Lamb, B. T. (2015). TREM2 deficiency eliminates TREM2+ inflammatory macrophages and ameliorates pathology in Alzheimer's disease mouse models. *The Journal of Experimental Medicine*, 212(3), 287–295. <https://doi.org/10.1084/jem.20142322>
- Jeon, S. B., Yoon, H. J., Park, S. H., Kim, I. H., & Park, E. J. (2008). Sulfatide, a major lipid component of myelin sheath, activates inflammatory responses as an endogenous stimulator in brain-resident immune cells. *Journal of Immunology*, 181(11), 8077–8087. <https://doi.org/10.4049/jimmunol.181.11.8077>
- Jones, L. L., Yamaguchi, Y., Stallcup, W. B., & Tuszynski, M. H. (2002). NG2 is a major chondroitin sulfate proteoglycan produced after spinal cord injury and is expressed by macrophages and oligodendrocyte progenitors. *The Journal of Neuroscience*, 22(7), 2792–2803. <https://doi.org/10.1523/JNEUROSCI.22-07-02792.2002>
- Jung, S., Aliberti, J., Graemmel, P., Sunshine, M. J., Kreutzberg, G. W., Sher, A., & Littman, D. R. (2000). Analysis of fractalkine receptor CX(3)CR1 function by targeted deletion and green fluorescent protein reporter gene insertion. *Molecular and Cellular Biology*, 20(11), 4106–4114. <https://doi.org/10.1128/mcb.20.11.4106-4114.2000>
- Kaushik, R., Lipachev, N., Matuszko, G., Kochneva, A., Dvoeglazova, A., Becker, A., ... Dityatev, A. (2020). Fine structure analysis of perineuronal nets in the ketamine model of schizophrenia. *The European Journal of Neuroscience*, in press. <https://doi.org/10.1111/ejn.14853>
- Keren-Shaul, H., Spinrad, A., Weiner, A., Matcovitch-Natan, O., Dvir-Szternfeld, R., Ulland, T. K., ... Amit, I. (2017). A unique microglia type associated with restricting development of Alzheimer's Disease. *Cell*, 169(7), 1276–1290. <https://doi.org/10.1016/j.cell.2017.05.018>
- Kettenmann, H., Hanisch, U. K., Noda, M., & Verkhratsky, A. (2011). Physiology of microglia. *Physiological Reviews*, 91(2), 461–553. <https://doi.org/10.1152/physrev.00011.2010>
- Kigerl, K. A., Gensel, J. C., Ankeny, D. P., Alexander, J. K., Donnelly, D. J., & Popovich, P. G. (2009). Identification of two distinct macrophage subsets with divergent effects causing either neurotoxicity or regeneration in the injured mouse spinal cord. *The Journal of Neuroscience*, 29(43), 13435–13444. <https://doi.org/10.1523/jneurosci.3257-09.2009>
- Kim, C., Cho, E. D., Kim, H. K., You, S., Lee, H. J., Hwang, D., & Lee, S. J. (2014). beta1-integrin-dependent migration of microglia in response to neuron-released alpha-synuclein. *Experimental & Molecular Medicine*, 46, e91. <https://doi.org/10.1038/emmm.2014.6>
- Kochlamazashvili, G., Henneberger, C., Bukalo, O., Dvoretzka, E., Senkov, O., Lievens, P. M., ... Dityatev, A. (2010). The extracellular matrix molecule hyaluronic acid regulates hippocampal synaptic plasticity by modulating postsynaptic L-type Ca(2+) channels. *Neuron*, 67(1), 116–128. <https://doi.org/10.1016/j.neuron.2010.05.030>
- Koenigsnecht-Talboo, J., Meyer-Luehmann, M., Parsadanian, M., Garcia-Alloza, M., Finn, M. B., Hyman, B. T., ... Holtzman, D. M. (2008). Rapid microglial response around amyloid pathology after systemic anti-Abeta antibody administration in PDAPP mice. *The Journal of Neuroscience*, 28(52), 14156–14164. <https://doi.org/10.1523/jneurosci.4147-08.2008>
- Krabbe, G., Halle, A., Matyash, V., Rinnenthal, J. L., Eom, G. D., Bernhardt, U., ... Heppner, F. L. (2013). Functional impairment of microglia coincides with Beta-amyloid deposition in mice with Alzheimer-like pathology. *PLoS One*, 8(4), e60921. <https://doi.org/10.1371/journal.pone.0060921>
- Krstic, D., Madhusudan, A., Doehner, J., Vogel, P., Notter, T., Imhof, C., ... Knuesel, I. (2012). Systemic immune challenges trigger and drive Alzheimer-like neuropathology in mice. *Journal of Neuroinflammation*, 9, 151. <https://doi.org/10.1186/1742-2094-9-151>
- Kwok, J. C., Dick, G., Wang, D., & Fawcett, J. W. (2011). Extracellular matrix and perineuronal nets in CNS repair. *Developmental Neurobiology*, 71(11), 1073–1089. <https://doi.org/10.1002/dneu.20974>
- Landel, V., Baranger, K., Virard, I., Llorid, B., Khrestchatsky, M., Rivera, S., ... Feron, F. (2014). Temporal gene profiling of the 5XFAD transgenic mouse model highlights the importance of microglial activation in Alzheimer's disease. *Molecular Neurodegeneration*, 9, 33. <https://doi.org/10.1186/1750-1326-9-33>
- Lee, H. J., Bian, S., Jakovcevski, I., Wu, B., Irintchev, A., & Schachner, M. (2012). Delayed applications of L1 and chondroitinase ABC promote recovery after spinal cord injury. *Journal of Neurotrauma*, 29(10), 1850–1863. <https://doi.org/10.1089/neu.2011.2290>
- Lin, R., Kwok, J. C., Crespo, D., & Fawcett, J. W. (2008). Chondroitinase ABC has a long-lasting effect on chondroitin sulphate glycosaminoglycan content in the injured rat brain. *Journal of Neurochemistry*, 104(2), 400–408. <https://doi.org/10.1111/j.1471-4159.2007.05066.x>
- Lue, L. F., Kuo, Y. M., Roher, A. E., Brachova, L., Shen, Y., Sue, L., ... Rogers, J. (1999). Soluble amyloid beta peptide concentration as a

- predictor of synaptic change in Alzheimer's disease. *The American Journal of Pathology*, 155(3), 853–862.
- Mantovani, A., Biswas, S. K., Galdiero, M. R., Sica, A., & Locati, M. (2013). Macrophage plasticity and polarization in tissue repair and remodelling. *The Journal of Pathology*, 229(2), 176–185. <https://doi.org/10.1002/path.4133>
- Marchetti, C., & Marie, H. (2011). Hippocampal synaptic plasticity in Alzheimer's disease: What have we learned so far from transgenic models? *Reviews in the Neurosciences*, 22(4), 373–402. <https://doi.org/10.1515/rns.2011.035>
- Meyer-Luehmann, M., Spires-Jones, T. L., Prada, C., Garcia-Alloza, M., de Calignon, A., Rozkalne, A., ... Hyman, B. T. (2008). Rapid appearance and local toxicity of amyloid-beta plaques in a mouse model of Alzheimer's disease. *Nature*, 451(7179), 720–724. <https://doi.org/10.1038/nature06616>
- Moffett, C. W., & Paden, C. M. (1994). Microglia in the rat neurohypophysis increase expression of class I major histocompatibility antigens following central nervous system injury. *Journal of Neuroimmunology*, 50(2), 139–151.
- Mohle, L., Israel, N., Paarmann, K., Krohn, M., Pietkiewicz, S., Muller, A., ... Dunay, I. R. (2016). Chronic toxoplasma gondii infection enhances beta-amyloid phagocytosis and clearance by recruited monocytes. *Acta Neuropathologica Communications*, 4, 25. <https://doi.org/10.1186/s40478-016-0293-8>
- Mohle, L., Mattei, D., Heimesaat, M. M., Bereswill, S., Fischer, A., Alutis, M., ... Wolf, S. A. (2016). Ly6C(hi) monocytes provide a link between antibiotic-induced changes in gut microbiota and adult hippocampal neurogenesis. *Cell Reports*, 15(9), 1945–1956. <https://doi.org/10.1016/j.celrep.2016.04.074>
- Montagne, A., Barnes, S. R., Sweeney, M. D., Halliday, M. R., Sagare, A. P., Zhao, Z., ... Zlokovic, B. V. (2015). Blood-brain barrier breakdown in the aging human hippocampus. *Neuron*, 85(2), 296–302. <https://doi.org/10.1016/j.neuron.2014.12.032>
- Neumann, J., Riek-Burchardt, M., Herz, J., Doeppner, T. R., Konig, R., Hutten, H., ... Gunzer, M. (2015). Very-late-antigen-4 (VLA-4)-mediated brain invasion by neutrophils leads to interactions with microglia, increased ischemic injury and impaired behavior in experimental stroke. *Acta Neuropathologica*, 129(2), 259–277. <https://doi.org/10.1007/s00401-014-1355-2>
- Nimmerjahn, A., Kirchhoff, F., & Helmchen, F. (2005). Resting microglial cells are highly dynamic surveillants of brain parenchyma in vivo. *Science*, 308(5726), 1314–1318. <https://doi.org/10.1126/science.1110647>
- Oakley, H., Cole, S. L., Logan, S., Maus, E., Shao, P., Craft, J., ... Vassar, R. (2006). Intraneuronal beta-amyloid aggregates, neurodegeneration, and neuron loss in transgenic mice with five familial Alzheimer's disease mutations: Potential factors in amyloid plaque formation. *The Journal of Neuroscience*, 26(40), 10129–10140. <https://doi.org/10.1523/jneurosci.1202-06.2006>
- Pai, M. C., & Yang, Y. C. (2013). Impaired translation of spatial representation in young onset Alzheimer's disease patients. *Current Alzheimer Research*, 10(1), 95–103. <https://doi.org/10.2174/156720513804871390>
- Palop, J. J., Chin, J., & Mucke, L. (2006). A network dysfunction perspective on neurodegenerative diseases. *Nature*, 443(7113), 768–773. <https://doi.org/10.1038/nature05289>
- Pannell, M., Economopoulos, V., Wilson, T. C., Kersemans, V., Isenegger, P. G., Larkin, J. R., ... Sibson, N. R. (2020). Imaging of translocator protein upregulation is selective for pro-inflammatory polarized astrocytes and microglia. *Glia*, 68(2), 280–297. <https://doi.org/10.1002/glia.23716>
- Paolicelli, R. C., Bolascho, G., Pagani, F., Maggi, L., Scianni, M., Panzanelli, P., ... Gross, C. T. (2011). Synaptic pruning by microglia is necessary for normal brain development. *Science*, 333(6048), 1456–1458. <https://doi.org/10.1126/science.1202529>
- Pendleton, J. C., Shablott, M. J., Gary, D. S., Belegu, V., Hurtado, A., Malone, M. L., & McDonald, J. W. (2013). Chondroitin sulfate proteoglycans inhibit oligodendrocyte myelination through PTP $\alpha$ . *Experimental Neurology*, 247, 113–121. <https://doi.org/10.1016/j.expneurol.2013.04.003>
- Pengas, G., Williams, G. B., Acosta-Cabronero, J., Ash, T. W., Hong, Y. T., Izquierdo-Garcia, D., ... Nestor, P. J. (2012). The relationship of topographical memory performance to regional neurodegeneration in Alzheimer's disease. *Frontiers in Aging Neuroscience*, 4, 17. <https://doi.org/10.3389/fnagi.2012.00017>
- Pizzorusso, T., Medini, P., Berardi, N., Chierzi, S., Fawcett, J. W., & Maffei, L. (2002). Reactivation of ocular dominance plasticity in the adult visual cortex. *Science*, 298(5596), 1248–1251. <https://doi.org/10.1126/science.1072699>
- Pothuizen, H. H., Davies, M., Aggleton, J. P., & Vann, S. D. (2010). Effects of selective granular retrosplenial cortex lesions on spatial working memory in rats. *Behavioural Brain Research*, 208(2), 566–575. <https://doi.org/10.1016/j.bbr.2010.01.001>
- Pyka, M., Wetzel, C., Aguado, A., Geissler, M., Hatt, H., & Faissner, A. (2011). Chondroitin sulfate proteoglycans regulate astrocyte-dependent synaptogenesis and modulate synaptic activity in primary embryonic hippocampal neurons. *The European Journal of Neuroscience*, 33(12), 2187–2202. <https://doi.org/10.1111/j.1460-9568.2011.07690.x>
- Raj, D., Yin, Z., Breur, M., Doorduyn, J., Holtman, I. R., Olah, M., ... Boddeke, E. (2017). Increased white matter inflammation in aging- and Alzheimer's disease brain. *Frontiers in Molecular Neuroscience*, 10, 206. <https://doi.org/10.3389/fnmol.2017.00206>
- Remington, L. T., Babcock, A. A., Zehntner, S. P., & Owens, T. (2007). Microglial recruitment, activation, and proliferation in response to primary demyelination. *The American Journal of Pathology*, 170(5), 1713–1724. <https://doi.org/10.2353/ajpath.2007.060783>
- Rice, R. A., Pham, J., Lee, R. J., Najafi, A. R., West, B. L., & Green, K. N. (2017). Microglial repopulation resolves inflammation and promotes brain recovery after injury. *Glia*, 65(6), 931–944. <https://doi.org/10.1002/glia.23135>
- Senkov, O., Sun, M., Weinhold, B., Gerardy-Schahn, R., Schachner, M., & Dityatev, A. (2006). Polysialylated neural cell adhesion molecule is involved in induction of long-term potentiation and memory acquisition and consolidation in a fear-conditioning paradigm. *The Journal of Neuroscience*, 26(42), 10888–10898. <https://doi.org/10.1523/jneurosci.0878-06.2006>
- Sholl, D. A. (1953). Dendritic organization in the neurons of the visual and motor cortices of the cat. *Journal of Anatomy*, 87(4), 387–406.
- Sierra, A., Encinas, J. M., Deudero, J. J., Chancey, J. H., Enikolopov, G., Overstreet-Wadiche, L. S., ... Maletic-Savatic, M. (2010). Microglia shape adult hippocampal neurogenesis through apoptosis-coupled phagocytosis. *Cell Stem Cell*, 7(4), 483–495. <https://doi.org/10.1016/j.stem.2010.08.014>
- Soleman, S., Filippov, M. A., Dityatev, A., & Fawcett, J. W. (2013). Targeting the neural extracellular matrix in neurological disorders. *Neuroscience*, 253, 194–213. <https://doi.org/10.1016/j.neuroscience.2013.08.050>
- Song, X. M., Yu, Q., Dong, X., Yang, H. O., Zeng, K. W., Li, J., & Tu, P. F. (2017). Aldose reductase inhibitors attenuate beta-amyloid-induced TNF-alpha production in microglia via ROS-PKC-mediated NF-kappaB and MAPK pathways. *International Immunopharmacology*, 50, 30–37. <https://doi.org/10.1016/j.intimp.2017.06.005>
- Steindler, D. A., & Cooper, N. G. (1986). Wheat germ agglutinin binding sites in the adult mouse cerebellum: Light and electron microscopic studies. *The Journal of Comparative Neurology*, 249(2), 170–185. <https://doi.org/10.1002/cne.902490205>
- Steinmetz, M. P., Horn, K. P., Tom, V. J., Miller, J. H., Busch, S. A., Nair, D., ... Silver, J. (2005). Chronic enhancement of the intrinsic growth capacity of sensory neurons combined with the degradation of inhibitory proteoglycans allows functional regeneration of sensory axons through the dorsal root entry zone in the mammalian spinal cord. *The Journal of Neuroscience*, 25(35), 8066–8076. <https://doi.org/10.1523/jneurosci.2111-05.2005>



- Stevens, B., Allen, N. J., Vazquez, L. E., Howell, G. R., Christopherson, K. S., Nouri, N., ... Barres, B. A. (2007). The classical complement cascade mediates CNS synapse elimination. *Cell*, 131(6), 1164–1178. <https://doi.org/10.1016/j.cell.2007.10.036>
- Sugar, J., Witter, M. P., van Strien, N. M., & Cappaert, N. L. (2011). The retrosplenial cortex: Intrinsic connectivity and connections with the (para) hippocampal region in the rat. An interactive connectome. *Frontiers in Neuroinformatics*, 5, 7. <https://doi.org/10.3389/fninf.2011.00007>
- Tan, R. H., Wong, S., Hodges, J. R., Halliday, G. M., & Hornberger, M. (2013). Retrosplenial cortex (BA 29) volumes in behavioral variant frontotemporal dementia and Alzheimer's disease. *Dementia and Geriatric Cognitive Disorders*, 35(3–4), 177–182. <https://doi.org/10.1159/000346392>
- Thinakaran, G., & Koo, E. H. (2008). Amyloid precursor protein trafficking, processing, and function. *The Journal of Biological Chemistry*, 283(44), 29615–29619. <https://doi.org/10.1074/jbc.R800019200>
- Tooyama, I., Kimura, H., Akiyama, H., & McGeer, P. L. (1990). Reactive microglia express class I and class II major histocompatibility complex antigens in Alzheimer's disease. *Brain Research*, 523(2), 273–280. [https://doi.org/10.1016/0006-8993\(90\)91496-4](https://doi.org/10.1016/0006-8993(90)91496-4)
- Tremblay, M. E., Lowery, R. L., & Majewska, A. K. (2010). Microglial interactions with synapses are modulated by visual experience. *PLoS Biology*, 8(11), e1000527. <https://doi.org/10.1371/journal.pbio.1000527>
- van de Haar, H. J., Jansen, J. F. A., van Osch, M. J. P., van Buchem, M. A., Muller, M., Wong, S. M., ... Backes, W. H. (2016). Neurovascular unit impairment in early Alzheimer's disease measured with magnetic resonance imaging. *Neurobiology of Aging*, 45, 190–196. <https://doi.org/10.1016/j.neurobiolaging.2016.06.006>
- Vegh, M. J., Heldring, C. M., Kamphuis, W., Hijazi, S., Timmerman, A. J., Li, K. W., ... van Kesteren, R. E. (2014). Reducing hippocampal extracellular matrix reverses early memory deficits in a mouse model of Alzheimer's disease. *Acta Neuropathologica Communications*, 2, 76. <https://doi.org/10.1186/s40478-014-0076-z>
- Ventura Ferreira, M. S., Bienert, M., Müller, K., Rath, B., Goecke, T., Opländer, C., ... Neuss, S. (2018). Comprehensive characterization of chorionic villi-derived mesenchymal stromal cells from human placenta. *Stem Cell Research & Therapy*, 9(1), 28. <https://doi.org/10.1186/s13287-017-0757-1>
- Wagner, M. J., Kim, T. H., Savall, J., Schnitzer, M. J., & Luo, L. (2017). Cerebellar granule cells encode the expectation of reward. *Nature*, 544 (7648), 96–100. <https://doi.org/10.1038/nature21726>
- Wang, Y., Cella, M., Mallinson, K., Ulrich, J. D., Young, K. L., Robinette, M. L., ... Colonna, M. (2015). TREM2 lipid sensing sustains the microglial response in an Alzheimer's disease model. *Cell*, 160(6), 1061–1071. <https://doi.org/10.1016/j.cell.2015.01.049>
- Yang, S., Cacquevel, M., Saksida, L. M., Bussey, T. J., Schneider, B. L., Aebischer, P., ... Spillantini, M. G. (2015). Perineuronal net digestion with chondroitinase restores memory in mice with tau pathology. *Experimental Neurology*, 265, 48–58. <https://doi.org/10.1016/j.expneurol.2014.11.013>
- Zhang, X., Ye, P., Wang, D., Liu, Y., Cao, L., Wang, Y., ... Zhu, C. (2019). Involvement of RhoA/ROCK signaling in A $\beta$ -induced chemotaxis, cytotoxicity and inflammatory response of microglial BV2 cells. *Cellular and Molecular Neurobiology*, 39(5), 637–650. <https://doi.org/10.1007/s10571-019-00668-6>
- Zhong, L., Wang, Z., Wang, D., Wang, Z., Martens, Y. A., Wu, L., ... Chen, X. F. (2018). Amyloid-beta modulates microglial responses by binding to the triggering receptor expressed on myeloid cells 2 (TREM2). *Molecular Neurodegeneration*, 13(1), 15. <https://doi.org/10.1186/s13024-018-0247-7>
- Zhu, Y., Hou, H., Rezai-Zadeh, K., Giunta, B., Ruscin, A., Gemma, C., ... Tan, J. (2011). CD45 deficiency drives amyloid-beta peptide oligomers and neuronal loss in Alzheimer's disease mice. *The Journal of Neuroscience*, 31(4), 1355–1365. <https://doi.org/10.1523/jneurosci.3268-10.2011>
- Zlokovic, B. V. (2005). Neurovascular mechanisms of Alzheimer's neurodegeneration. *Trends in Neurosciences*, 28(4), 202–208. <https://doi.org/10.1016/j.tins.2005.02.001>

## SUPPORTING INFORMATION

Additional supporting information may be found online in the Supporting Information section at the end of this article.

**How to cite this article:** Stoyanov S, Sun W, Düsedau HP, et al. Attenuation of the extracellular matrix restores microglial activity during the early stage of amyloidosis. *Glia*. 2021;69: 182–200. <https://doi.org/10.1002/glia.23894>